**N. Jb. Miner. Abh. (J. Min. Geochem.) 191/3 (2014), 257–276** **Article**
Published online May 2014; published in print June 2014

# $^{40}$Ar-$^{39}$Ar age, petrography and geochemistry of the Yoncayolu Metamorphic Rocks (NE Turkey): Subduction-related metamorphism under greenschist facies conditions

Mehmet Ali Gücer and Zafer Aslan

With 13 figures and 6 tables

**Abstract:** The Yoncayolu Metamorphic Rocks (YMR), exposed in the Sakarya zone (Erzincan, NE Turkey), consists mainly of greenschist rocks which are chlorite schists, muscovite-chlorite schists, metabasic rocks and lesser extent of pyhllites and calc-schists. All YMR are fine-grained, weakly foliated and often cut by quartz veins. The common mineral assemblage is chlorite+albite+epidote+quartz ± clinozoisite ± actinolite ± opaques. Geochemically, protoliths of the YMR resemble calc-alkaline volcanic arc rocks. The YMR have high contents of large ion lithophile elements (LILEs) and low contents of high field strength elements (HFSEs) similar to mid-ocean ridge basalt (MORB). $(La/Lu)_{CN}$ values are between 0.26 and 6.16. The REE patterns show slight or no Eu anomalies ($Eu_{CN}/Eu^*$ of 0.48 to 1.13), suggesting minor plagioglase fractionation. $^{40}$Ar-$^{39}$Ar dating on plagioclases from the metabasic samples of the YMR gave ages of 100.8 ± 3.4 Ma (Albian) and 94.1 ± 3.3 Ma (Cenomanian), suggesting that metamorphism was related to the closure of the Neo-Tethyan Ocean. Metamorphism took place during subduction of the Neo-Tethyan Ocean between ~90–70 Ma. Chlorite geothermometry yielded a temperature of 320–350 °C and a pressure around 4 kbar. All these findings lend support for greenschist facies metamorphic conditions during the formation of the YMR.

Key words: Yoncayolu Metamorphic Rocks, NE Turkey, $^{40}$Ar-$^{39}$Ar age, greenschist facies, chlorite thermobarometry.

## 1. Introduction

Turkey is part of the Alpine orogenic belt which formed by the collision of Laurasia with Gondwana in the Late Cretaceous-EarlyTertiary (Şengör & Yilmaz 1981, Şengör et al. 1985). It can be divided into four main geological units: the Sakarya zone, the Anatolide–Tauride Block, the Intra-Pontide suture zone, and the Assyrian–Zagros suture zone (Okay & Tüysüz 1999). The Sakarya zone, which extends from the northwest to the northeast of Turkey to the İzmir–Ankara–Erzincan suture zone, comes into direct contact with the Anatolide–Taurides block in the Eastern Pontides. The Sakarya zone contains metamorphic basement rocks that are overlain by sediments and volcanic rocks (Okay & Şahintürk 1997, Okay & Tüysüz 1999, Okay & Göncüoğlu 2004). The metamorphic rocks can be divided into two groups according to their ages: Devonian-Late Carboniferous and Late Cretaceous. The Devonian-Late Carboniferous rocks were metamorphosed under high temperature/low pressure conditions. The resulting gneisses, amphibolites, migmatites and ultramafic rocks were cut by Paleozoic granitoids such as the Pulur massif in the east of the Sakarya zone (Okay & Satir 2000, Topuz et al. 2004).

Late Cretaceous metamorphic rocks are exposed along the İzmir–Ankara–Erzincan suture within the Sakarya zone. These rocks, that are mainly composed of volcanogenic sediments (Okay 1984), have undergone greenschist or blueschist facies metamorphism and were formed during subduction between the Pontides and Anatolide–Taurides blocks (Okay & Tüysüz 1999) in a volcanic arc or back-arc basin (Okay & Şahintürk 1997, Okay & Tüysüz 1999). Low-grade metamorphism in the Sakarya zone is generally assumed to have occurred during the Upper Cretaceous (Okay et al. 2006). Likewise, the age of low pressure-medium temperature (LP-MT) blueschist metamorphism in the whole region between eastern Turkey to western Iran is estimated to have occurred between 95 and 75 Ma (Rolland et al. 2009). In the Assyrian–Zagros suture zone, the age of metamor-


www.schweizerbart.de
DOI: 10.1127/0077-7757/2014/0260 0077-7757/2014/0260 $ 4.75

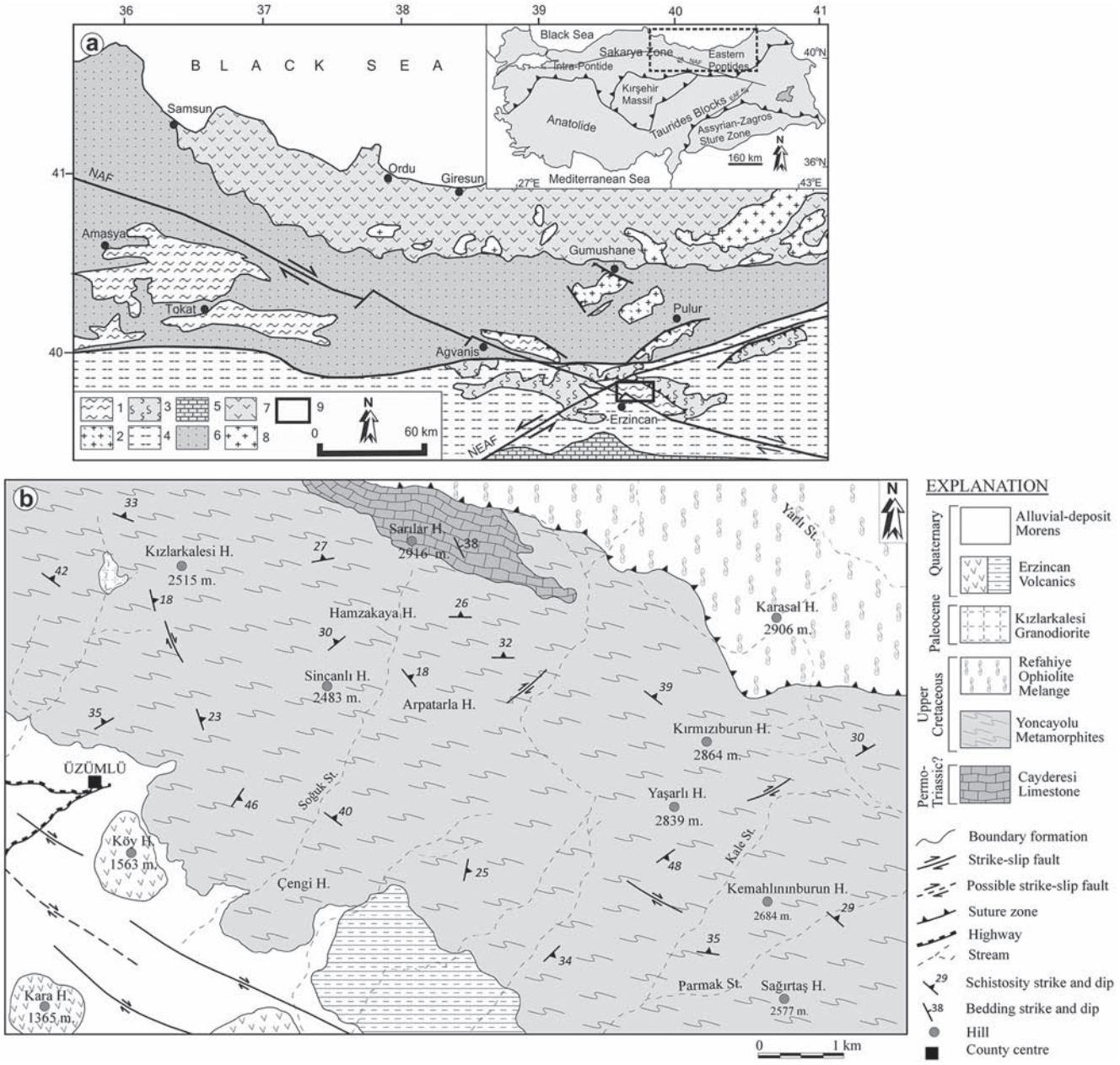


**Fig. 1. (a)** Main tectonic features and tectonic zones of NE Turkey (simplified from Eyüboglu et al. 2006). **(1)** Palaeozoic metamorphic basement, **(2)** Palaeozoic granites, **(3)** Serpentinite, **(4)** undifferentiated Mesozoic and Cenozoic rocks, **(5)** platform carbonates, **(6)** mainly Mesozoic sedimentary rocks, **(7)** Cretaceous and Eocene arc volcanic rocks, **(8)** Late Cretaceous and Eocene arc granites, **(9)** study area. NAF: North Anatolian Fault; NEAF: Northeast Anatolian Fault. **(b)** Geological map of the study area (from Gücer 2008).

phism has been dated between 79–67 Ma (Oberhänsli et al. 2011).

The Yoncayolu metamorphic rocks (YMR) (Fig. 1a) are exposed in the Üzümlü area (Erzincan) at the southern border of the Eastern Pontides and along the İzmir–Ankara–Erzincan suture in the eastern part of the Sakarya zone (e.g. Şengör & Yilmaz 1981, Göncüoğlu & Turhan 1983). In previous studies, a Permo-Triassic age was assigned to the YMR (Bektaş 1981, Okay & Şahintürk 1997, Sarifakioglu et al. 2009). Although other massifs in the region have been studied (e.g. Ketin 1966, Bektaş 1981, Okay 1984, Okay & Şahintürk 1997, Altinkaynak 2001, Topuz et al. 2004, 2011, Sarifakioglu et al. 2009) there has been insufficient detailed work on the petrography, geochemistry, metamorphism and age of the YMR. The aim of this work, therefore, is to provide new mineralogical, geochemical and geochronological data for the YMR.

## 2. Geological setting and local geology

On the basis of lithology and facies-type Paleozoic basement rocks of the Eastern Pontides can be grouped into two units, one in the north, and one in the south (Okay & Şahintürk 1997). In the northern zone, the rocks are Devonian–Carboniferous in age and have been metamorphosed to chlorite schist, chlorite–sericite schist, chlorite–amphibole–quartz–albite schist, muscovite–biotite–quartz schist, gneiss and marble (Topuz et al. 2007). This metamorphic basement is covered by Liassic volcanogenic sediments and Upper Jurassic–Lower Cretaceous limestones that outcrop over a large area (Okay & Şahintürk 1997, Aslan 2005). In the southern zone, the rocks are of Permo–Triassic age and have been metamorphosed into phyllite, chlorite–sericite schist, muscovite–sericite–quartz schist, calc-schist, quartzite, gneiss and amphibolite (Topuz et al. 2004).

The YMR cover an area of ~60 km$^2$ (Fig. 1b) and are composed of widespread greenschists rocks comprising chlorite schists, muscovite-chlorite schists, metabasics, rare pyhllites and calc-schists. All these rocks are frequently cut by 5–50 cm thick quartz veins and were metamorphosed under greenschist facies P-T conditions. Chlorite schists occur at the base and successively upwards there are muscovite-chlorite schists, phyllites, metabasics and calc-schists. Chlorite schists are the most widespread lithology in the study area. They are yellowish in colour and have a clearly visible foliation oriented parallel to the original bedding planes. Foliation dips at 20–50°, generally towards the N and NE. The phyllites are fine-grained, weakly foliated, and locally graphitic. Micaschists are restricted to the central part of the lithological succession. Lithological horizons are approximately parallel to each other, but their thicknesses are variable. In some places, the rocks have lost their original characteristics and are characterised by metamorphic textures. Along the northern boundary, the YMR are tectonically overlain by the Refahiye ophiolitic mélange (Bektaş 1981).

The Late Paleocene (60.7 ± 4.9 Ma) Kızlarkalesi granodioritic intrusion (Aslan et al. 2011) intruded into the chlorite schists (Fig. 1b). Epidote hornfels containing epidote, garnet hematite, limonite, silica and calcite formed locally at the contact with this intrusion in the Kızlarkalesi Hills, north of Üzümlü. Apart from foliation, other structures observed include small-scale isoclinal folds.

The Cayderesi limestone unconformably underlies the YMR and consists of dolomite and recrystallised limestone (Gücer 2008). The limestone unit is 50–150 m thick and represents a shallow, low-energy pelagic marine facies. As a result of intense fracturing and recrystallization the rocks have lost many of their original features.

The Refahiye ophiolitic mélange tectonically overlies the YMR and the Cayderesi limestone. It consists of peridotite, dunite, serpentinite, amphibolite and gabbro (Şengör & Yilmaz 1981, Sarifakioglu et al. 2009). The Refahiye ophiolite was formed in the earliest stages of island arc development in a supra-subduction forearc tectonic setting, i.e., similar to other Jurassic–Cretaceous Eastern Mediterranean ophiolites (Sarifakioglu et al. 2009). The ophiolitic rocks were emplaced as nappes during the Lower Campanian–Lower Maastrichtian (Sarifakioglu et al. 2009). Okay & Şahintürk (1997) suggested that the Refahiye ophiolite and the volcanic arc in the Eastern Pontides are both related to the northwards subduction of the Neo-Tethyan Ocean beneath the Eastern Pontides continental margin. The Quaternary Erzincan volcanics unconformably overlie all the other units. The youngest rocks in the study area are alluvium and slope debris material.

## 3. Materials and methods

One hundred samples from the YMR were analysed petrographically with a polarizing microscope (Nikon Eclipse E400 POL). Based on petrographic observations, 33 samples were selected for major, trace and rare earth elements (REEs) analysis. Analyses of whole-rock major elements, trace elements and REEs were carried out using inductively coupled plasma–atomic emission spectrometry (ICP–AES) and inductively coupled plasma–mass spectrometry (ICP–MS) at ACME Analytical Laboratories Ltd., Vancouver, Canada. Major- and trace-element compositions were determined by ICP–AES after 0.2 g of whole-rock powder was fused with 1.5 g $LiBO_2$ and dissolved in 100 ml of 5 % $HNO_3$. REEs content were analysed by ICP–MS after dissolving 0.25 g samples of rock powder. Loss on ignition (LOI) is defined as the difference in weight before and after ignition at 1000 °C. The detection limits range from 0.01 to 0.1 wt% for major oxides, 0.1 to 10 ppm for trace elements, and 0.01 to 0.5 ppm for the REEs.

The mineral compositions of plagioclase, chlorite, muscovite, amphibole, epidote and pyroxene were determined on carbon-coated polished sections using a JEOL JXA-8900 L electron microprobe at Earth & Planetary Sciences Department, McGill University, Canada. The counting time for individual elements was 20 s and the sample current was 20 nA. The results were processed with Sigma Plot and Grapher 5.0 computer programs.

$^{40}$Ar-$^{39}$Ar incremental dating was performed at the Actlabs in Canada. Samples wrapped in Al foil were loaded in evacuated and sealed quartz vials with K and Ca

salts and packets of LP-6 biotite muscovite interspersed with the samples were used as flux monitor. The samples were irradiated in the VEK-11 carrier of the VVR-K research reactor for 48 hours. The flux monitors were placed between every two samples, thereby allowing precise determination of the flux gradients within the tube. After the flux monitors were run, J values were then calculated for each sample, using the measured flux gradient. LP-6 biotite has an assumed age of 128.1 Ma. The neutron gradient did not exceed 0.5 % of the sample size. $^{40}Ar$-$^{39}Ar$ step heating experiments were accomplished in a quartz reactor heated by an external furnace. Released gases were purified by exposure to two Ti-getters and two SAES getters. The Ar isotope composition was measured on a Micromass 5400 static mass spectrometer. $^{40}Ar$ blank (measured at 1200 °C) did not exceed $n*10^{-10}$ STP.

## 4. Results

### 4.1. Rock types and mineral compositions

The YMR consist of mainly chlorite schists and lesser extent pyhllites, muscovite-chlorite schists, metabasic rocks and calc-schists. According to point counting, mineral

**Table 1.** Mineral content (%) for representative rock samples of the YMR.

| | Mineral content (%) | | | | |
|---|---|---|---|---|---|
| Sample No. | M-1 | M-7A | M-17 | M-30 | M-32 |
| | Phyllite | Chlorite schist | Chlorite schist | Chlorite schist | Metabasite |
| Quartz | 75 | 60 | 16 | 35 | |
| Plagioclase | < 1 | 30 | 5 | 6 | 60 |
| K-feldspar | | 7 | | < 1 | |
| Amphibole | < 1 | | | | 39 |
| Sericite | | 3 | < 1 | | 1 |
| Biotite | | | | < 1 | |
| Chlorite | 8 | < 1 | 10 | 50 | |
| Epidote | 5 | | 60 | 1 | |
| Garnet | | | 8 | | |
| Calcite | 12 | < 1 | 1 | 6 | |
| Clay mineral | | | < 1 | | |
| Apatite | | | < 1 | < 1 | |
| Rutile | < 1 | < 1 | | < 1 | < 1 |
| Magnetite | | | < 1 | 1 | < 1 |
| Hematite | < 1 | | | 1 | |

**Table 2.** Major mineral assemblages and textures of the YMR.

| Sample No | Rocks type | Mineral paragenesis | Texture |
|---|---|---|---|
| M2 | Epidote-chlorite-albite schist | ep+chl+ab+cal ± opq | Lepidoporphyroblastic |
| M3 | Epidote-chlorite schist | ep+chl+cal+ab+ser+± op | Granoblasticlepidoblastic |
| M4 | Albite-chlorite schist | qtz+chl+ab+cal+ser ± op | Lepidogranoblastic |
| M5 | Chlorite schist | qtz+chl+ep ± hem ± op | Lepidoblastic |
| M6 | Albite-epidote-chlorite schist | qtz+cal+chl+ab+ep ± op | Lepidogranoblastic |
| M7 A, B | Muscovite-quartz schist | mus+qtz+kfs+chl ± op | Lepidogranoblastic |
| M11 | Chlorite schist | chl+qtz+kfs ± op | Lepidoblastic |
| M13 | Epidote-chlorite schist | ep+czo+pl+chl+kfs ± mag ± ap | Lepidogranoblastic |
| M17 | Epidote-chlorite schist | ep+czo+pl+chl+kfs ± mag ± ap | Lepidogranoblastic |
| M24 | Amphibole-chlorite schist | act+hbl+kfs+cal+ser ± opq | Lepidogranoblastic |
| M30 | Chlorite schist | chl+kfs+pl+or+ep+cal+mag+hem ± ap | Lepidoblastic |
| MT2 | Chlorite schist | chl+ab+ser+cal+ep ± op | Lepidoblastic |
| MT3 | Epidote-calcite-chlorite schist | ep+chl+cal+ser+alb ± op | Granolepidoblastic |
| M7D | Muscovite-chlorite schist | ms+chl+cal+ab+ser ± op | Lepidoporphyroblastic |
| M10B | Muscovite-quartz-chlorite schist | ms+chl+kfs+ab+ser+cal+kfs ± op | Lepidogranoporphyroblastic |
| M15 | Muscovite-chlorite schist | ms+chl+kfs+ab+ser ± op | Lepidoporphyroblastic |
| M32 | Metabasite | pl+am (act+hbl)+ser+mag | Granoblastic |
| M1 | Phyllite | ser+qtz+chl+cal+ep ± am ± hem ± op | Lepidoblastic |
| M18 | Calc schist | cal ± op | Granoblastic |
| M19 | Calc schist | cal ± op | Granoblastic |

contents of selected YMR samples (n = 6) are presented in Table 1. The results of a detailed mineralogical–petrographical investigation of 24 samples are presented in Table 2.

### *4.1.1 Greenschist rocks*

#### Chlorite schist

The chlorite schists are fine grained rocks with clearly visible foliation and often cut by veins of quartz, calcite and epidote. They consist of epidote–chlorite–albite schists, epidote–clinozoisite–chlorite schists, albite–epidote–chlorite schists, albite–chlorite schists, epidote–sericite–chlorite schists and quartz–albite–calcite–chlorite schists. In the chlorite schists, the most common mineral assemblage is chlorite+albite+epidote+quartz ± clinozoisite ± actinolite ± opaque minerals (Table 2). The textures are porphyroblastic, lepidoblastic, lepidogranoblastic and -porphyroblastic. Phenocrysts or clasts of albite and aggregates of quartz (recrystallised clasts) are set in a fine-grained matrix of chlorite and minor quartz. Albite is generally altered and locally present as relict phenocrysts from the parent rock (Fig. 2a).

Generally, plagioclases are altered and made up of albite ($An_{0.17-1.59}$ $Ab_{98.26-99.69}$ $Or_{0.05-0.30}$) (Table 3). Some relict phenocrysts of plagioclase contain iron oxides. All plagioclases show albite twinning and/or oscillatory zoning. The compositions of the plagioclases (An < 7) and their association with chlorite is typical of greenschist facies rocks. Fine-grained quartz, which makes up part of the matrix, occurs as flattened and granulated grains, suggesting shearing. The accompanying chlorite-rich layers are contorted, also suggesting shear deformation. Chlorite occurs in layers which define the rock fabric and generally forms tiny grains. The strongly pleochroic green chlorite-rich layers are deformed and wrapped around feldspar phenocrysts.

The total FeO contents of chlorites are between 13 and 26 wt%, and the MgO contents range between 14 and 23 wt% (Table 4). Epidote occurs as fine- and coarse-grained aggregates, some of which appear to have crystallised at the expense of actinolite. Clinozoisite with anomalous blue interference colours forms a replace-

**Table 3.** Representative microprobe analyses of plagioclase from the YMR.

| Mineral | Plagioclase | | | | | | | |
|---|---|---|---|---|---|---|---|---|
| Sample No. | M2a | M2b | M2c | M10Ba | M10Bb | M7Aa | M7Ab | M7Ac |
| Rock type | Chlorite schist | Chlorite schist | Chlorite schist | Muscovite-Chlorite schist | Muscovite-Chlorite schist | Chlorite schist | Chlorite schist | Chlorite schist |
| $SiO_2$ | 68.74 | 68.38 | 68.17 | 68.00 | 68.06 | 67.99 | 67.88 | 68.09 |
| $TiO_2$ | 0.036 | 0.000 | 0.004 | 0.006 | 0.000 | 0.020 | 0.013 | 0.000 |
| $Al_2O_3$ | 19.61 | 19.58 | 19.57 | 19.81 | 19.76 | 19.88 | 19.98 | 19.86 |
| $Cr_2O_3$ | 0.000 | 0.022 | 0.000 | 0.011 | 0.001 | 0.000 | 0.011 | 0.006 |
| FeO | 0.063 | 0.071 | 0.152 | 0.068 | 0.075 | 0.000 | 0.046 | 0.039 |
| MgO | 0.000 | 0.000 | 0.009 | 0.001 | 0.000 | 0.000 | 0.009 | 0.000 |
| CaO | 0.036 | 0.083 | 0.051 | 0.148 | 0.153 | 0.131 | 0.318 | 0.340 |
| BaO | 0.008 | 0.000 | 0.000 | 0.015 | 0.007 | 0.000 | 0.027 | 0.015 |
| $Na_2O$ | 11.69 | 11.69 | 11.69 | 11.71 | 11.66 | 11.72 | 11.59 | 11.62 |
| $K_2O$ | 0.024 | 0.024 | 0.025 | 0.029 | 0.014 | 0.041 | 0.053 | 0.028 |
| TOTAL | 100.21 | 99.85 | 99.67 | 99.80 | 99.74 | 99.78 | 99.93 | 100.00 |
| Si | 2.9943 | 2.9908 | 2.9885 | 2.9787 | 2.9816 | 2.9773 | 2.9709 | 2.9769 |
| Ti | 0.0012 | 0.0000 | 0.0001 | 0.0002 | 0.0000 | 0.0007 | 0.0004 | 0.0000 |
| Al | 1.0070 | 1.0095 | 1.0110 | 1.0226 | 1.0206 | 1.0262 | 1.0306 | 1.0234 |
| Fe | 0.0023 | 0.0026 | 0.0056 | 0.0025 | 0.0027 | 0.0000 | 0.0017 | 0.0014 |
| Mg | 0.0000 | 0.0000 | 0.0006 | 0.0000 | 0.0000 | 0.0000 | 0.0006 | 0.0000 |
| Ca | 0.0017 | 0.0039 | 0.0024 | 0.0069 | 0.0072 | 0.0061 | 0.0149 | 0.0159 |
| Ba | 0.0001 | 0.0000 | 0.0000 | 0.0003 | 0.0001 | 0.0000 | 0.0005 | 0.0003 |
| Na | 0.9875 | 0.9917 | 0.9939 | 0.9945 | 0.9907 | 0.9951 | 0.9834 | 0.9849 |
| K | 0.0014 | 0.0013 | 0.0014 | 0.0016 | 0.0008 | 0.0023 | 0.0030 | 0.0015 |
| Ab | 99.69 | 99.48 | 99.62 | 99.15 | 99.20 | 99.16 | 99.21 | 98.26 |
| An | 0.17 | 0.39 | 0.24 | 0.69 | 0.72 | 0.61 | 1.49 | 1.59 |
| Or | 0.14 | 0.13 | 0.14 | 0.16 | 0.08 | 0.23 | 0.30 | 0.15 |
| *Calculations are based on 8 oxygen atoms* | | | | | | | | |

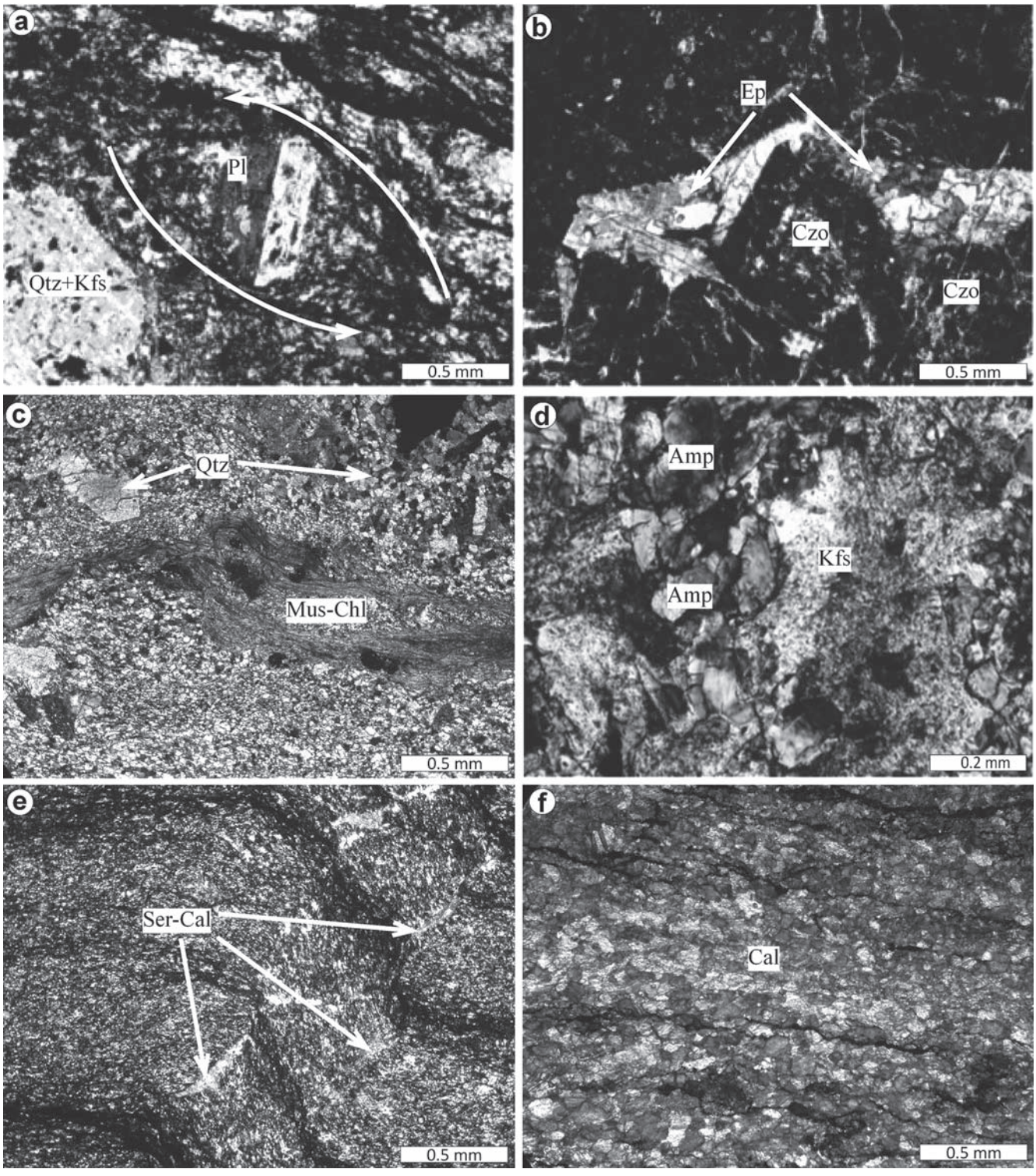


**Fig. 2.** Thin section microphotographs showing textural features of the YMR. **(a)** Rotation of relict phenocrystal of plagioclase in chlorite schist, **(b)** epidote and clinozoisite in chlorite schist, **(c)** muscovite and chlorite in lepidoblastic quartz micaschist, **(d)** amphibole and highly altered K-feldspar in metabasic rock, **(e)** lepidoblastic texture in phyllite, **(f)** granoblastic calc-schist. (Ser: sericite, Cal: calcite, Pl: plagioclase, Qtz: quartz, Kfs: K-feldspat, Mus: muscovite, Chl: chlorite, Ep: epidote, Czo: clinozoisite, Amp: amphibole).

**Table 4.** Representative microprobe analyses of muscovite, epidote, amphibole, pyroxene and chlorite from the YMR.

| Mineral | Muscovite | | | Epidote | Amphibole | | | | Pyroxene | Chlorite | | |
|---|---|---|---|---|---|---|---|---|---|---|---|---|
| Sample No. | M10B | M7A | M15 | M13 | M23 | M32 | M32 | M32 | M23 | M2 | M17 | M17 |
| Rock type | Muscovite-Chlorite schist | Muscovite-Chlorite schist | Muscovite-Chlorite schist | Chlorite-schist | Chlorite schist | Metabasite | Metabasite | Metabasite | Muscovite-Chlorite schist | Chlorite schist | Chlorite schist | Chlorite schist |
| $SiO_2$ | 46.20 | 47.64 | 49.71 | 37.20 | 55.47 | 52.26 | 51.06 | 50.65 | 51.85 | 25.91 | 28.31 | 28.21 |
| $TiO_2$ | 0.178 | 0.123 | 0.069 | 0.086 | 0.022 | 0.508 | 0.639 | 0.365 | 0.191 | 0.033 | 0.002 | 0.016 |
| $Al_2O_3$ | 32.91 | 28.94 | 27.22 | 20.85 | 1.14 | 3.63 | 4.08 | 4.59 | 2.15 | 19.94 | 21.19 | 21.07 |
| $Cr_2O_3$ | 0.000 | 0.000 | 0.000 | 0.000 | 0.020 | 0.094 | 0.059 | 0.355 | 0.043 | 0.027 | 0.043 | 0.054 |
| FeO | 2.97 | 3.93 | 2.34 | 14.62 | 10.25 | 13.41 | 13.80 | 13.89 | 11.17 | 26.97 | 13.47 | 13.51 |
| MgO | 0.765 | 2.02 | 3.66 | 0.103 | 17.50 | 16.22 | 15.70 | 15.56 | 16.02 | 14.67 | 23.73 | 23.88 |
| MnO | 0.004 | 0.014 | 0.030 | 0.327 | 0.228 | 0.309 | 0.307 | 0.314 | 0.302 | 0.457 | 0.315 | 0.283 |
| CaO | 0.046 | 0.000 | 0.039 | 22.75 | 12.48 | 11.16 | 11.21 | 11.08 | 17.70 | 0.067 | 0.098 | 0.060 |
| $Na_2O$ | 0.768 | 0.275 | 0.138 | 0.000 | 0.244 | 0.551 | 0.592 | 0.724 | 0.251 | 0.013 | 0.000 | 0.006 |
| $K_2O$ | 10.52 | 11.56 | 11.75 | 0.000 | 0.008 | 0.033 | 0.075 | 0.054 | 0.000 | 0.003 | 0.008 | 0.005 |
| TOTAL | 94.34 | 94.51 | 94.95 | 95.93 | 97.36 | 98.17 | 97.53 | 97.58 | 99.68 | 88.09 | 87.17 | 87.09 |
| Si | 6.2750 | 6.5267 | 6.7196 | 3.2580 | 7.8640 | 7.3325 | 7.2464 | 7.1816 | 1.9381 | 5.490 | 5.606 | 5.596 |
| Ti | 0.0182 | 0.0127 | 0.0070 | 0.0057 | 0.0023 | 0.0536 | 0.0682 | 0.0389 | 0.0054 | 0.005 | 0.000 | 0.002 |
| Al | 5.2685 | 4.6733 | 4.3365 | 2.1526 | 0.1898 | 0.6005 | 0.6823 | 0.7674 | 0.0948 | 4.985 | 4.954 | 4.932 |
| Cr | 0.0000 | 0.0000 | 0.0000 | 0.0000 | 0.0022 | 0.0104 | 0.0066 | 0.0398 | 0.0013 | 0.005 | 0.007 | 0.008 |
| $Fe^{2+}$ | 0.3368 | 0.4507 | 0.2649 | 1.0708 | 1.0006 | 0.4680 | 0.5430 | 0.4692 | 0.3491 | 4.790 | 2.230 | 2.241 |
| Mg | 0.1549 | 0.4121 | 0.7366 | 0.0134 | 3.6986 | 3.3924 | 3.3214 | 3.2879 | 0.8924 | 4.636 | 7.005 | 7.061 |
| Mn | 0.0005 | 0.0016 | 0.0034 | 0.0243 | 0.0274 | 0.0367 | 0.0369 | 0.0377 | 0.0095 | 0.082 | 0.053 | 0.048 |
| Ca | 0.0067 | 0.0000 | 0.0056 | 2.1352 | 1.8958 | 1.6776 | 1.7051 | 1.6827 | 0.7089 | 0.015 | 0.021 | 0.013 |
| Na | 0.2023 | 0.0730 | 0.0362 | 0.0000 | 0.0671 | 0.1499 | 0.1629 | 0.1990 | 0.0182 | 0.011 | 0.000 | 0.005 |
| K | 1.8218 | 2.0203 | 2.0268 | 0.0000 | 0.0014 | 0.0059 | 0.0136 | 0.0098 | 0.0000 | 0.002 | 0.004 | 0.003 |
| $Al^{IV}$ | 1.7250 | 1.4733 | 1.2804 | – | 0.1360 | 0.6005 | 0.6823 | 0.7674 | – | 2.510 | 2.394 | 2.404 |
| $Al^{VI}$ | 3.5435 | 3.2001 | 3.0561 | – | 0.0539 | 0.0000 | 0.0000 | 0.0000 | – | 2.475 | 2.560 | 2.528 |
| $Mg/(Mg+Fe^{2+})$ | 0.3150 | 0.4776 | 0.7355 | – | 0.7871 | 0.8788 | 0.8595 | 0.8751 | – | 0.492 | 0.766 | 0.765 |

Calculations are basen on 22 oxygen atoms for muscovite, 13 for epidote, 23 for amphibole, 8 for pyroxene and 28 for chlorite.

ment product of feldspar phenocrysts. The centres of most clinozoisites are semi-isotropic and brown in colour, probably representing earlier Fe-stained clays within the feldspars. Fine-grained magnetite and hematite are disseminated through the matrix, and also occur in thin layers parallel to the chlorite-rich layers. The amount of sericite increases with the amount of epidote; on the contrary, it decreases with increasing amount of clinozoisite (Fig. 2b). Rutile and apatite are accessory minerals.

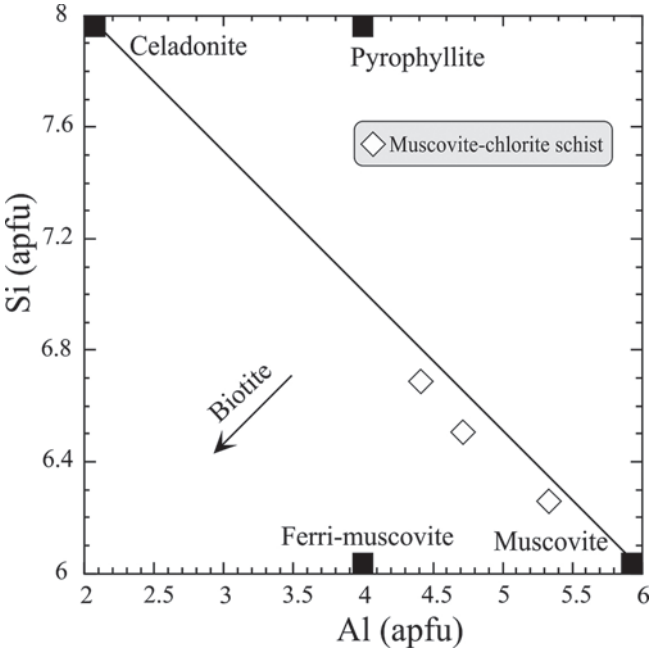


**Fig. 3.** Si versus-$Al_{tot}$ discrimination diagram for white mica.

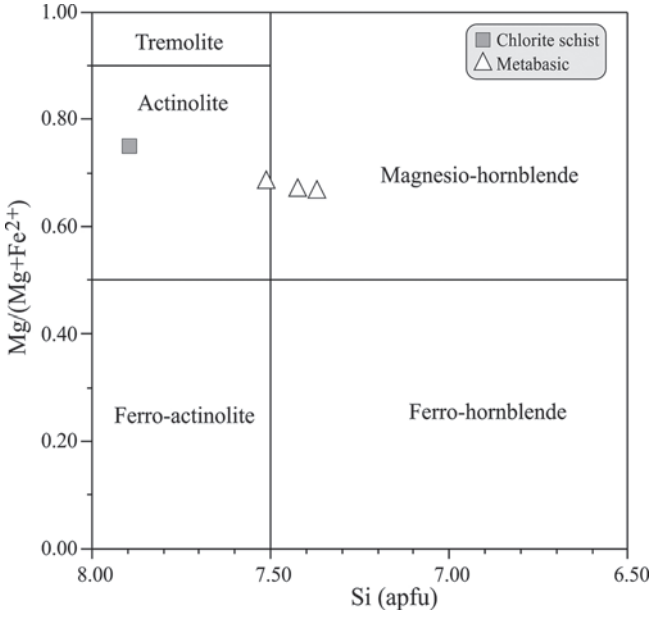


**Fig. 4.** Chemical classification (Leake et al. 1997) of amphiboles from the YMR.

**Muscovite-chlorite schist**

The muscovite-chlorite schist has a lepidoblastic texture, and the typical mineral assemblage is muscovite+quartz+chlorite ± sericite (Table 2; Fig. 2c). Muscovite occurs in contorted stringers, and is associated with chlorite. Muscovite has $X_{Mg}$ = 0.32–0.74 (Table 4). Although most minerals in the muscovite-chlorite schists are usually fine grained (< 0.1 mm), some reach sizes of 0.5 mm. The orientations of white mica and chlorite define the schistosity. In the Si versus – $Al_{tot}$ diagram (Fig. 3), the minerals plot close to the muscovite compositional field.

**Metabasic rocks**

Textures of the metabasics are granoblastic, nematoblastic and nematogranoblastic (Table 2). Their mineral assemblage is albite (An < 7)+chlorite+epidote+amphibole ± calcite ± sericite ± magnetite. Some rotated plagioclase porphyroblasts have pressure shadows of quartz and chlorite. The anhedral to subhedral plagioclases are sericitised and altered. Pleochroic green amphibole also occurs as part of the matrix, and is intergrown with feldspar (Fig. 2d). Amphibole glomerocrysts are up to 2 mm long, and a few small veins consisting of fine-grained needles of actinolite and quartz cross cut the rock fabric. Some of the amphiboles are relics from the original rocks, but others are formed by alteration of pyroxene during greenschist facies metamorphism. In the metabasics, the relict amphibole phenocrysts vary from subhedral to anhedral. Their $Mg/(Mg+Fe^{2+})$ ratios range from 0.79 to 0.88 (Table 4). According to the Si versus – $Mg/(Mg+Fe^{2+})$ discrimination diagram of Leake et al. (1997), the amphibole compositions plot into the magnesio-hornblende and actinolite fields (Fig. 4). The magnesio-hornblende is generally colourless or light green, and the actinolite occurs as acicular crystals. A few very small grains of magnetite are disseminated throughout the rock.

Sericite occurs as a very fine-grained alteration product of plagioclase. Accessory minerals are magnetite and rutile.

*4.1.2. Phyllite and calc-schist*

Greenish and bluish phyllite is altered and generally contains a weak foliation. The main mineral assemblage in the phyllite is sericite+chlorite+quartz ± calcite ± epidote ± albite ± opaque minerals. The rocks exhibit lepidoblastic textures (Table 2; Fig. 2e). Very fine-grained phyllite consists of sericite, fine-grained quartz, stringers of fine-grained chlorite, calcite, clusters of epidote aggregates and plagioclase. The sericites are very fine-grained and oriented parallel to the schistosity. Fine-grained,

**Table 5.** Major, trace and REE element composition of the YMR (major elements in wt%, trace elements and REE in ppm).

| | Chlorite schist | | | | | | | | | | | |
|---|---|---|---|---|---|---|---|---|---|---|---|---|
| Sample | M2 | M3 | M13 | M8 | M17 | M17B | M14 | M7A | M7B | M7C | M27 | M20 |
| $SiO_2$ | 50.74 | 57.82 | 50.72 | 73.19 | 44.99 | 49.28 | 46.36 | 76.77 | 75.33 | 77.2 | 74.32 | 48.28 |
| $TiO_2$ | 0.87 | 1.06 | 0.43 | 0.35 | 0.17 | 0.53 | 0.27 | 0.23 | 0.25 | 0.24 | 0.4 | 0.5 |
| $Al_2O_3$ | 15.86 | 13.08 | 21.2 | 12.96 | 21.7 | 21.81 | 21.37 | 9.48 | 9.77 | 9.59 | 12.16 | 18.6 |
| $Fe_2O_3$* | 9.62 | 12.66 | 7.51 | 3.17 | 6.3 | 7.83 | 6.82 | 2.05 | 2.26 | 2.4 | 3.31 | 10.72 |
| MgO | 3.83 | 4.62 | 2.33 | 2.28 | 5.43 | 2.4 | 4.97 | 0.86 | 1.03 | 1.04 | 1.22 | 6.64 |
| CaO | 7.67 | 4.18 | 10.69 | 0.63 | 14.58 | 11.25 | 11.97 | 2.46 | 3 | 2.13 | 0.71 | 7.95 |
| $Na_2O$ | 4.99 | 2.68 | 2.97 | 5.67 | 1.33 | 3.02 | 2.2 | 4.41 | 4.49 | 4.35 | 5.68 | 2 |
| $K_2O$ | 0.13 | 0.42 | 0.52 | 0.09 | bdl | 0.51 | 0.17 | 0.45 | 0.36 | 0.36 | 0.67 | 0.34 |
| MnO | 0.17 | 0.28 | 0.12 | 0.05 | 0.14 | 0.13 | 0.13 | 0.08 | 0.1 | 0.08 | 0.04 | 0.15 |
| $P_2O_5$ | 0.09 | 0.08 | 0.05 | 0.06 | 0.01 | 0.05 | 0.02 | 0.06 | 0.06 | 0.06 | 0.09 | 0.04 |
| $Cr_2O_3$ | 0.002 | 0.001 | bdl | 0.006 | 0.01 | 0.001 | 0.009 | bdl | bdl | bdl | bdl | 0.002 |
| LOI | 5.9 | 3 | 3.3 | 1.6 | 5.2 | 3.2 | 5.6 | 3.2 | 3.4 | 2.6 | 1.3 | 4.8 |
| TOTAL | 99.87 | 99.88 | 99.85 | 100.06 | 99.9 | 100.01 | 99.89 | 100.05 | 100.05 | 100.04 | 99.9 | 100.03 |
| Ba | 34.3 | 88.8 | 115.1 | 14.3 | 7.9 | 107.3 | 26 | 82.3 | 69.4 | 73.8 | 200.3 | 55.1 |
| Co | 24.2 | 26.8 | 18.2 | 17 | 22.3 | 18.3 | 22.5 | 2.1 | 2.2 | bdl | bdl | 12 |
| Cs | bdl | 0.2 | 0.1 | 12 | 0.1 | 0.2 | 0.1 | 0.3 | 0.2 | 10 | 15 | 43 |
| Ni | bdl | bdl | bdl | 5.1 | 32 | bdl | 10 | bdl | bdl | 2.3 | 3.7 | 31.6 |
| Sc | 37 | 49 | 27 | bdl | 33 | 27 | 35 | 10 | 10 | 0.2 | 0.3 | 0.2 |
| Ga | 15.9 | 15.5 | 16.2 | 10.6 | 15.3 | 17.2 | 15.5 | 7.5 | 7.8 | 7.8 | 10.8 | 14.4 |
| Hf | 1 | 1.1 | 0.5 | 1.9 | bdl | 0.5 | bdl | 2 | 2.4 | 2.3 | 2.7 | bdl |
| Nb | 0.8 | 0.5 | dla | 1.1 | bdl | 0.5 | bdl | 0.9 | 1 | 0.9 | 1 | bdl |
| Rb | 1.8 | 6.7 | 7.3 | 1.1 | 0.5 | 7 | 2 | 7.6 | 6.1 | 6 | 5 | 2.5 |
| Sr | 302 | 190 | 266 | 43 | 308 | 296 | 253 | 60 | 69 | 60 | 48 | 212 |
| Ta | 0.1 | bdl | bdl | bdl | bdl | bdl | bdl | 0.1 | 0.1 | 0.1 | 0.1 | bdl |
| Th | 0.8 | 0.3 | 0.5 | 0.9 | 0.1 | 0.3 | bdl | 0.6 | 0.4 | 0.5 | 0.4 | bdl |
| U | 0.3 | 0.2 | 0.2 | 0.2 | 0.1 | 0.2 | 0.1 | 0.3 | 0.3 | 0.2 | 0.4 | 0.1 |
| V | 401 | 368 | 281 | 42 | 146 | 334 | 196 | 10 | 9 | 9 | 29 | 329 |
| W | 0.4 | 0.7 | 0.3 | 0.5 | 0.4 | 0.4 | 0.3 | 0.3 | 0.2 | 0.4 | 0.1 | bdl |
| Zr | 30.1 | 23.4 | 14.1 | 50.7 | 6.3 | 14.4 | 5.6 | 63.1 | 69.5 | 65.3 | 73 | 12.9 |
| Y | 16 | 24.3 | 9.5 | 24.9 | 4.7 | 9.3 | 5.7 | 29 | 33.1 | 33.2 | 37.9 | 9.3 |
| La | 4.6 | 2.2 | 2.6 | 2.1 | 4.6 | 2.9 | 1.6 | 4 | 4.5 | 4.2 | 4.8 | 1.1 |
| Ce | 10.2 | 4.3 | 4.9 | 5.2 | 2.5 | 5.1 | 2.3 | 10.9 | 12.1 | 11.6 | 10.8 | 2.2 |
| Pr | 1.32 | 0.7 | 0.67 | 0.75 | 0.35 | 0.69 | 0.34 | 1.78 | 1.95 | 1.86 | 1.73 | 0.36 |
| Nd | 6.7 | 4.5 | 3.8 | 3.8 | 1.8 | 3.5 | 1.7 | 9.2 | 9.8 | 10.3 | 10.4 | 2.4 |
| Sm | 1.9 | 2 | 1.2 | 1.3 | 0.5 | 1.1 | 0.6 | 3.2 | 3.5 | 3.4 | 3.6 | 0.8 |
| Eu | 0.62 | 0.69 | 0.39 | 0.43 | 0.21 | 0.41 | 0.23 | 0.78 | 0.9 | 0.88 | 0.93 | 0.31 |
| Gd | 2.41 | 2.9 | 1.31 | 2.25 | 0.67 | 1.33 | 0.76 | 3.75 | 4.1 | 4.06 | 4.57 | 1.26 |
| Tb | 0.45 | 0.64 | 0.25 | 0.54 | 0.13 | 0.26 | 0.14 | 0.77 | 0.81 | 0.83 | 0.96 | 0.27 |
| Dy | 2.65 | 3.89 | 1.56 | 3.55 | 0.76 | 1.67 | 0.9 | 4.9 | 5.1 | 4.99 | 5.75 | 1.57 |
| Ho | 0.53 | 0.82 | 0.31 | 0.8 | 0.15 | 0.33 | 0.17 | 0.95 | 1.01 | 1.05 | 1.2 | 0.33 |
| Er | 1.74 | 2.71 | 1.01 | 2.96 | 0.49 | 1.06 | 0.61 | 2.99 | 3.57 | 3.6 | 3.93 | 1.14 |
| Tm | 0.27 | 0.38 | 0.17 | 0.46 | 0.08 | 0.17 | 0.1 | 0.49 | 0.59 | 0.62 | 0.62 | 0.2 |
| Yb | 1.7 | 2.84 | 1.05 | 2.97 | 0.45 | 1.06 | 0.58 | 3.29 | 3.81 | 4.12 | 4.23 | 1.17 |
| Lu | 0.27 | 0.41 | 0.18 | 0.51 | 0.08 | 0.17 | 0.09 | 0.48 | 0.57 | 0.6 | 0.65 | 0.17 |
| $(La/Lu)_{CN}$ | 1.83 | 0.57 | 1.55 | 0.44 | 6.16 | 1.83 | 1.91 | 0.89 | 0.85 | 0.75 | 0.79 | 0.69 |
| Eu/Eu* | 0.88 | 0.87 | 1.50 | 0.76 | 1.14 | 1.04 | 1.04 | 0.69 | 0.73 | 0.72 | 0.70 | 0.94 |
| Mg# | 28.48 | 26.74 | 23.68 | 41.83 | 46.29 | 23.46 | 42.15 | 29.55 | 31.31 | 30.23 | 26.93 | 38.25 |

pleochroic green chlorites form a series of parallel layers, some of which wrap around aggregates of epidote, calcite and quartz. Together with sericite, chlorite defines the weak schistosity. The chlorite-rich layers contain fine-grained epidote and calcite. The quartz grains are somewhat flattened and, together with the narrow chlorite layers, define the rock fabric. Some calcites are twisted and extend parallel to the schistosity. Fine-grained calcites are disseminated throughout the quartz-rich matrix, and small domains of quartz, epidote and calcite form boudins surrounded by chlorite-rich layers. Small grains of hematite are found in the interstices of calcite.

The main minerals of the laminar and schistose calc-schists are calcite and dolomite. Light yellow and grey coloured calc-schists have granoblastic textures (Table 2; Fig. 2f) and are cut by quartz and calcite veins.

**Table 5.** Continued

| | Chlorite schist | | | | | | | | | | | |
|---|---|---|---|---|---|---|---|---|---|---|---|---|
| Sample | M21 | M20B | M23 | M4 | M24A | M11 | M24B | M9B | M30 | M30A | M6 | M6B |
| $SiO_2$ | 45.22 | 60.27 | 49.85 | 49.4 | 71.41 | 71.96 | 64.64 | 71.16 | 47.85 | 49.21 | 58.6 | 63.49 |
| $TiO_2$ | 0.44 | 0.5 | 0.45 | 0.86 | 0.25 | 0.37 | 0.61 | 0.52 | 0.51 | 0.71 | 0.58 | 0.42 |
| $Al_2O_3$ | 14.12 | 15.14 | 17.51 | 15.37 | 9.68 | 13.34 | 14.7 | 14.11 | 17.89 | 16.96 | 15.28 | 15 |
| $Fe_2O_3$* | 9.8 | 7.08 | 9.49 | 12.21 | 3.39 | 4.5 | 4.94 | 3.03 | 10.43 | 12.39 | 7.24 | 5.93 |
| MgO | 4.24 | 3.3 | 7.37 | 5.16 | 4.37 | 1.68 | 3.7 | 2.63 | 8.22 | 7.21 | 2.74 | 2.42 |
| CaO | 10.34 | 6.38 | 7.69 | 5.9 | 3.64 | 0.28 | 1.63 | 0.42 | 2.71 | 2.65 | 5.68 | 3.96 |
| $Na_2O$ | 5.08 | 1.31 | 2.34 | 3.5 | 4.66 | 6.14 | 3.16 | 5.78 | 3.17 | 4.49 | 3.51 | 3.84 |
| $K_2O$ | 0.67 | 1.97 | 0.4 | 0.15 | 0.65 | 0.05 | 3.41 | 0.31 | 2.26 | 0.57 | 0.75 | 0.88 |
| MnO | 0.11 | 0.12 | 0.15 | 0.3 | 0.2 | 0.05 | 0.13 | 0.04 | 0.19 | 0.2 | 0.24 | 0.12 |
| $P_2O_5$ | 0.01 | 0.08 | 0.05 | 0.05 | 0.05 | 0.06 | 0.23 | 0.05 | 0.03 | 0.04 | 0.09 | 0.07 |
| $Cr_2O_3$ | 0.006 | 0.002 | 0.008 | 0.003 | bdl | bdl | bdl | 0.002 | 0.002 | 0.001 | bdl | bdl |
| LOI | 9.9 | 3.7 | 4.6 | 7 | 1.6 | 1.5 | 2.7 | 2 | 6.8 | 5.6 | 5.3 | 3.9 |
| TOTAL | 99.94 | 99.85 | 99.92 | 99.91 | 99.9 | 99.94 | 99.85 | 100.06 | 100.06 | 100.04 | 100.01 | 100.04 |
| Ba | 10.7 | 198.7 | 38.2 | 23.4 | 124.3 | 16.1 | 506.7 | 61.8 | 122 | 35.7 | 111.3 | 173.7 |
| Co | 12 | 6 | 18 | bdl | bdl | bdl | bdl | bdl | 10 | bdl | 7 | bdl |
| Cs | 33 | 28 | 39 | 47 | 10 | 14 | 15 | 24 | 38 | 43 | 29 | 23 |
| Ni | 26.4 | 14.9 | 30.1 | 36.5 | 6.5 | 4.8 | 5 | 7.2 | 29.3 | 32.3 | 15.2 | 13.5 |
| Sc | 0.5 | 1.2 | 0.2 | 0.1 | 0.4 | bdl | 3.1 | 0.1 | 1 | 0.3 | 0.3 | 0.3 |
| Ga | 8.9 | 13.9 | 14 | 16.7 | 5.9 | 12 | 14.9 | 10.9 | 15.2 | 17.7 | 15 | 13.1 |
| Hf | bdl | 1.3 | 0.6 | bdl | 2.1 | 2 | 3.2 | 2.1 | 0.5 | 0.7 | 1.2 | 1.7 |
| Nb | bdl | 0.9 | bdl | bdl | 1.4 | 1.1 | 3.5 | 0.9 | bdl | bdl | 0.8 | 0.9 |
| Rb | 11.8 | 19.8 | 4.4 | 2 | 7.9 | bdl | 46.8 | 3.6 | 17.3 | 4 | 11.3 | 12.2 |
| Sr | 29 | 447 | 86 | 117 | 81 | 35 | 188 | 33 | 41 | 56 | 103 | 151 |
| Ta | bdl | 0.1 | bdl | bdl | 0.1 | 0.1 | 0.2 | 0.1 | bdl | bdl | bdl | 0.1 |
| Th | bdl | 0.7 | 0.1 | 0.1 | 1.6 | 0.5 | 5.1 | 0.3 | 0.1 | 0.1 | 0.5 | 1.1 |
| U | 0.1 | 0.3 | 0.2 | 0.1 | 0.6 | 0.2 | 1.2 | 0.2 | bdl | 0.1 | 0.3 | 0.4 |
| V | 326 | 190 | 296 | 441 | 29 | 49 | 42 | 20 | 289 | 394 | 159 | 129 |
| W | 1.9 | 0.1 | 0.7 | 0.2 | 0.2 | 0.2 | 0.6 | 0.9 | 0.4 | 0.4 | 0.3 | 0.3 |
| Zr | 10.2 | 36.9 | 14.7 | 11 | 68.1 | 48.9 | 97 | 58.6 | 13.6 | 19 | 34.1 | 45.9 |
| Y | 8.6 | 18.6 | 9.9 | 15.2 | 16.9 | 18.3 | 24.5 | 37.9 | 14.4 | 14 | 22.1 | 19.2 |
| La | 0.5 | 4.9 | 1.9 | 1.3 | 6.6 | 1.9 | 21.4 | 2.9 | 1 | 1.2 | 3.9 | 4.5 |
| Ce | 1 | 9.6 | 4.3 | 1.8 | 13.8 | 3.3 | 41.8 | 7.7 | 2.7 | 2.4 | 8.3 | 10.2 |
| Pr | 0.22 | 1.33 | 0.64 | 0.39 | 1.76 | 0.62 | 4.91 | 1.31 | 0.48 | 0.45 | 1.31 | 1.5 |
| Nd | 1.4 | 7.3 | 3.3 | 2.6 | 8.9 | 3.4 | 22 | 8.2 | 3.2 | 2.7 | 5.8 | 7.8 |
| Sm | 0.5 | 2.1 | 1.1 | 1.1 | 2.6 | 1.2 | 4.8 | 3.1 | 1.5 | 1.1 | 2.3 | 2.3 |
| Eu | 0.18 | 0.6 | 0.37 | 0.52 | 0.42 | 0.3 | 1.28 | 0.75 | 0.54 | 0.44 | 0.7 | 0.6 |
| Gd | 1.01 | 2.44 | 1.38 | 1.79 | 2.7 | 1.6 | 4.29 | 4.27 | 1.98 | 1.67 | 2.86 | 2.4 |
| Tb | 0.2 | 0.5 | 0.26 | 0.38 | 0.5 | 0.4 | 0.76 | 0.96 | 0.43 | 0.36 | 0.6 | 0.51 |
| Dy | 1.43 | 3.21 | 1.57 | 2.42 | 2.68 | 2.8 | 3.97 | 6 | 3 | 2.19 | 3.55 | 3.08 |
| Ho | 0.29 | 0.57 | 0.32 | 0.5 | 0.49 | 0.61 | 0.74 | 1.22 | 0.55 | 0.47 | 0.71 | 0.62 |
| Er | 0.94 | 1.97 | 1.07 | 1.72 | 1.63 | 2.23 | 2.49 | 4.12 | 1.75 | 1.55 | 2.42 | 2.12 |
| Tm | 0.15 | 0.28 | 0.17 | 0.24 | 0.27 | 0.35 | 0.39 | 0.65 | 0.28 | 0.25 | 0.35 | 0.32 |
| Yb | 0.89 | 2.05 | 1.1 | 1.65 | 1.54 | 2.58 | 2.66 | 4.24 | 1.8 | 1.59 | 2.49 | 2.21 |
| Lu | 0.14 | 0.32 | 0.19 | 0.24 | 0.25 | 0.41 | 0.4 | 0.63 | 0.25 | 0.24 | 0.38 | 0.36 |
| $(La/Lu)_{CN}$ | 0.38 | 1.64 | 1.7 | 0.58 | 2.83 | 0.50 | 5.73 | 0.49 | 0.43 | 0.54 | 1.10 | 1.34 |
| Eu/Eu* | 0.77 | 0.81 | 0.92 | 1.13 | 0.48 | 0.66 | 0.86 | 0.63 | 0.96 | 0.99 | 0.83 | 0.78 |
| Mg# | 30.20 | 31.79 | 43.71 | 29.71 | 56.31 | 27.18 | 42.82 | 46.47 | 44.08 | 36.79 | 27.45 | 28.98 |

## 4.2. Geochemistry

Thirty-three representative samples of the YMR, including 27 chlorite schists, 2 muscovite-chlorite schists, 2 calc-schists, 1 metabasite and 1 phyllite have been analysed for their whole-rock major element, trace element, and REE contents (Table 5). The analytical data are plotted in diagrams used to infer the nature of the protoliths. The $SiO_2$, $Al_2O_3$, $Fe_2O_3$, MgO, CaO and $Na_2O$ contents are highly variable. The chlorite schists contain 45–79 wt% $SiO_2$, 8.73–21.81 wt% $Al_2O_3$, 0.76–8.22 wt% MgO, 1.72–12.66 wt% $Fe_2O_3$, 0.28–14.58 wt% CaO, 1.31–6.20 wt% $Na_2O$ and 0.05–3.41 wt% $K_2O$. This variability results from the diverse composition of the original rocks.

**Table 5.** Continued

| | Cholorite schist | | | Muscovite-schist | | Phyllite | Metabasite | Calc schist | |
|---|---|---|---|---|---|---|---|---|---|
| | | | | chlorite schist | | | | | |
| Sample | MT1 | MT2 | MT3 | M15 | M10B | M1 | M32 | M18 | M19 |
| $SiO_2$ | 48.85 | 49.24 | 51.41 | 79.36 | 70.96 | 67.78 | 56.3 | 1.42 | 0.85 |
| $TiO_2$ | 0.72 | 0.52 | 0.93 | 0.22 | 0.31 | 0.86 | 0.43 | 0.01 | 0.02 |
| $Al_2O_3$ | 19.33 | 18.81 | 16.72 | 8.73 | 13.99 | 11.76 | 14.05 | 0.35 | 0.28 |
| $Fe_2O_3$* | 10.97 | 9.3 | 12.43 | 1.72 | 3.27 | 7.02 | 7.44 | 0.18 | 0.24 |
| MgO | 3.12 | 4.76 | 6.04 | 0.76 | 1.13 | 2.45 | 7.13 | 0.67 | 2.31 |
| CaO | 11.84 | 4.05 | 3.72 | 2.09 | 1.84 | 2.16 | 6.6 | 54.59 | 52.83 |
| $Na_2O$ | 1.86 | 6.2 | 4.65 | 3.98 | 4.95 | 4.73 | 5.46 | 0.04 | 0.01 |
| $K_2O$ | 0.1 | 0.8 | 0.06 | 0.45 | 0.93 | 0.06 | 0.47 | 0.05 | 0.09 |
| MnO | 0.16 | 0.17 | 0.16 | 0.07 | 0.06 | 0.1 | 0.14 | 0.01 | 0.02 |
| $P_2O_5$ | 0.11 | 0.07 | 0.07 | 0.05 | 0.06 | 0.1 | 0.04 | 0.02 | bdl |
| $Cr_2O_3$ | 0.001 | bdl | bdl | bdl | bdl | bdl | 0.058 | bdl | 0.001 |
| LOI | 2.9 | 6.1 | 3.7 | 2.5 | 2.4 | 2.9 | 1.9 | 42.6 | 43.3 |
| TOTAL | 99.97 | 100.03 | 99.9 | 99.92 | 99.91 | 99.92 | 100.03 | 99.95 | 99.95 |
| Ba | 27.7 | 205.6 | 19.4 | 100.4 | 216.2 | 11.4 | 51.7 | 7.9 | 3.9 |
| Co | 20 | 24 | 18 | 1.7 | bdl | 8.5 | 62 | bdl | bdl |
| Cs | 32 | 32 | 42 | 0.3 | 14 | bdl | 35 | bdl | bdl |
| Ni | 27.4 | 26.1 | 30 | bdl | 4.4 | bdl | 30.8 | bdl | bdl |
| Sc | 0.1 | 0.2 | bdl | 9 | 0.4 | 30 | 0.2 | bdl | 0.1 |
| Ga | 19.6 | 14.2 | 15.2 | 7.1 | 11.4 | 12.7 | 10.5 | 0.6 | 0.5 |
| Hf | 0.7 | bdl | 0.6 | 1.6 | 1.7 | 1.5 | 1 | bdl | bdl |
| Nb | 0.6 | 0.5 | bdl | 0.8 | 1 | 0.7 | 0.8 | bdl | bdl |
| Rb | 1.3 | 13.4 | bdl | 7.6 | 13.4 | 0.7 | 5.4 | 1.2 | 0.9 |
| Sr | 915 | 59 | 161 | 59 | 59 | 33 | 183 | 223 | 254 |
| Ta | bdl | bdl | bdl | bdl | 0.1 | 0.1 | | bdl | bdl |
| Th | 1 | 0.5 | bdl | 0.4 | 1.2 | 0.2 | 0.4 | 0.2 | 0.1 |
| U | 0.3 | 0.2 | 0.1 | 0.2 | 0.4 | 0.2 | 0.2 | 1.3 | 1.6 |
| V | 379 | 268 | 374 | 12 | 57 | 32 | 195 | 9 | 19 |
| W | 0.4 | 0.2 | 1.4 | 0.2 | 0.4 | 0.6 | 0.2 | bdl | 0.1 |
| Zr | 19.1 | 17.1 | 14.8 | 55.9 | 49.9 | 36.2 | 32.3 | 2.1 | 2.7 |
| Y | 13.6 | 11.1 | 16.7 | 29.1 | 18.1 | 29 | 15.4 | 2.1 | 0.9 |
| La | 5.3 | 2.9 | 0.7 | 4.2 | 6.6 | 4 | 2 | 2 | 1.7 |
| Ce | 10.9 | 6.4 | 1.9 | 11.4 | 13.5 | 5.6 | 4.5 | 1.1 | 1.4 |
| Pr | 1.49 | 0.92 | 0.4 | 1.78 | 1.77 | 1.01 | 0.66 | 0.22 | 0.16 |
| Nd | 7.2 | 4.7 | 2.7 | 9.6 | 8.2 | 5.6 | 3.7 | 1 | 0.5 |
| Sm | 1.9 | 1.3 | 1.3 | 3.1 | 2.2 | 2.5 | 1.2 | 0.3 | 0.2 |
| Eu | 0.67 | 0.35 | 0.53 | 0.79 | 0.6 | 0.88 | 0.43 | bdl | bdl |
| Gd | 2.09 | 1.55 | 2.02 | 3.86 | 2.39 | 3.54 | 1.88 | 0.29 | 0.15 |
| Tb | 0.39 | 0.31 | 0.44 | 0.77 | 0.49 | 0.73 | 0.41 | 0.04 | 0.02 |
| Dy | 2.25 | 1.92 | 2.81 | 4.89 | 2.87 | 4.68 | 2.44 | 0.23 | 0.13 |
| Ho | 0.44 | 0.36 | 0.58 | 0.98 | 0.57 | 0.95 | 0.57 | bdl | bdl |
| Er | 1.46 | 1.2 | 1.97 | 2.96 | 1.96 | 3.24 | 1.77 | 0.14 | 0.08 |
| Tm | 0.22 | 0.18 | 0.29 | 0.48 | 0.32 | 0.48 | 0.26 | bdl | bdl |
| Yb | 1.43 | 1.21 | 1.98 | 3.21 | 2.17 | 3.24 | 1.56 | 0.07 | bdl |
| Lu | 0.2 | 0.18 | 0.29 | 0.47 | 0.34 | 0.48 | 0.26 | 0.02 | 0.01 |
| $(La/Lu)_{CN}$ | 3.00 | 1.73 | 0.26 | 0.96 | 2.08 | 0.89 | 0.82 | 10.38 | 17.65 |
| Eu/Eu* | 1.03 | 0.75 | 1.00 | 0.69 | 0.80 | 0.90 | 0.87 | – | – |
| Mg# | 22.14 | 33.85 | 32.70 | 30.65 | 25.68 | 25.87 | 48.94 | 78.82 | 90.59 |

$Fe_2O_3$* is total iron, LOI: loss on ignition, Mg# = 100× MgO/(MgO+$Fe^2O^3$), $(La/Lu)_{CN} = (La/La_{CN})/(Lu/Lu_{CN})$,
$Eu/Eu^* = (Eu/Eu_{CN})/\sqrt{(Sm/Sm_{CN})*(Gd/Gd_{CN})}$ , Chondrite (CN) values from Sun & McDonough 1989, bdl: below detection limit.

Except calc-schists and phyllites, the protoliths of the YMR were mostly magmatic in origin, as can bee seen from the Al–S–F triangular diagram (Fig. 5). In the Zr/$TiO_2$ versus – Nb/Y diagram, the greenschist rocks fall into the andesite, andesite/basalt, and subalkaline basalt fields (Fig. 6a). In the La versus -Yb diagram, (Fig. 6b) most chlorite schists, metabasic rocks and the phyllite sample plot in the tholeiitic field, a few in the transitional field. Harker variation diagrams indicate the trends for the major and trace elements: CaO, $Fe_2O_3$, MgO, $Al_2O_3$, $TiO_2$,

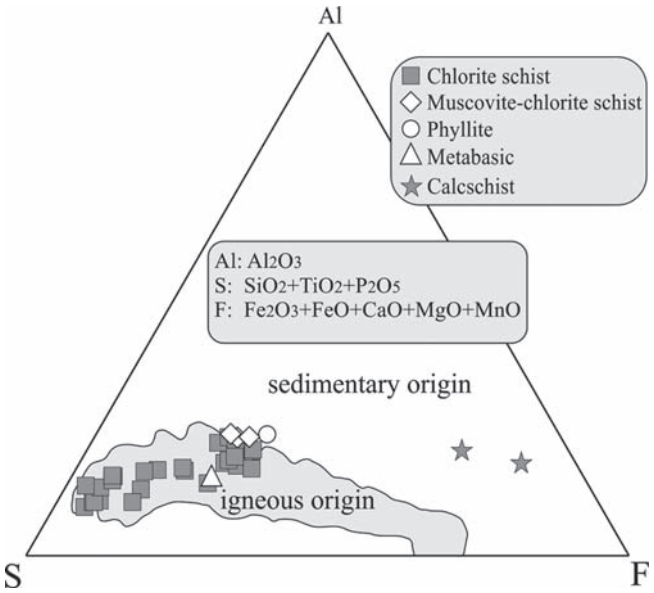


**Fig. 5.** Al-S-F triangular diagram (AYAN 1973).

Sr and Ni decrease with increasing $SiO_2$ content, whereas $Na_2O$, Y, Zr, $P_2O_5$, Th and Nb increase; $K_2O$ and Rb show irregular variations (Fig. 7). These element trends might reflect the variability of the protolith composition. Decrease in CaO, $Fe_2O_3$ and $Al_2O_3$ concentrations may indicate the importance of plagioclase and pyroxene fractionation in the original unmetamorphosed rocks. Na and K are highly mobile elements in greenschists, and their concentrations might have been modified during metamorphism. In the Hf/3-Th-Nb/16 ternary diagram, the greenschist rock samples of the YMR plot in the field of volcanic-arc basalt (Fig. 8) revealing that they could have been generated above an active subduction zone.

In Fig. 9a, the trace element contens of the YMR are normalized to N-type mid-ocean ridge basalt (N-MORB). The large-ion lithophile elements (LILEs), Rb, Ba, Th and K, are generally enriched; conversely, the high field strength elements (HFSEs), Ta, Nb, Zr and Ti, are depleted. The concentrations of other trace elements, such as Sr, Ta, Ce, Hf, Sm, Y and Yb, are similar to MORB. The enrichment of Th, K and Rb is attributed to the contribution of crustal material, and the negative Nb anomaly emphasises their formation in a subduction zone environment. Chondrite-normalised REE concentrations of the YMR are given in Fig. 9b. The YMR have $(La/Lu)_{CN}$ = 0.26–6.16, and $(Eu/Eu^*)_{CN}$ = 0.48–1.13. Eu anomalies are chiefly controlled by plagioclase fractionation. The REE patterns of the chlorite schists, metabasites and the phyllite sample are approximately parallel to each other.

## 4.3. Ar-Ar dating

Metabasic rocks of the YMR contain relict plagioclase minerals suitable for $^{40}Ar$-$^{39}Ar$ dating. Measured isotopic ratios and calculated ages of the two plagioclase seperates from sample M32 are given in Table 6 and the age spectrum, Ca/K spectrum and inverse isochron diagram is shown in Fig. 10. These plagioclase yielded plateau ages of 100.8 ± 3.4 Ma (Albian) and 94.1 ± 3.3 (Cenomanian). On the inverse isochron plots, data points form linear

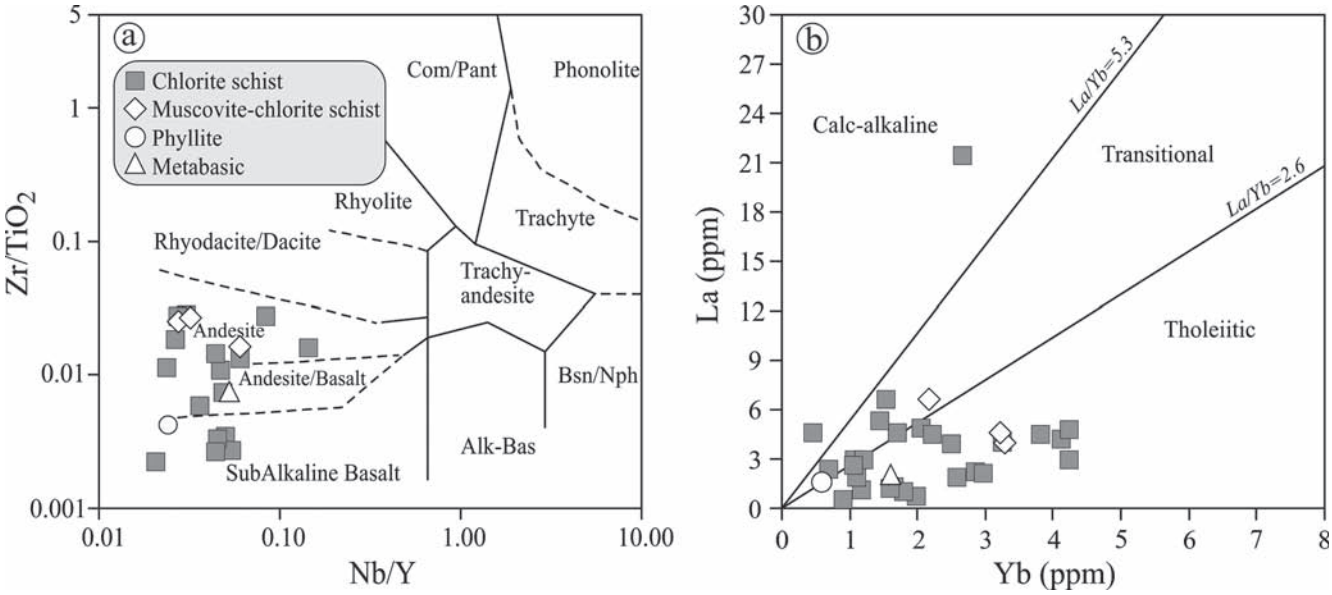


**Fig. 6. (a)** $Zr/TiO_2$ versus-Nb/Y diagram (WINCHESTER & FLOYD 1977) and **(b)** La (ppm) vs. Yb (ppm) classification diagram for YMR samples (ROSS & BÉDARD 2009).

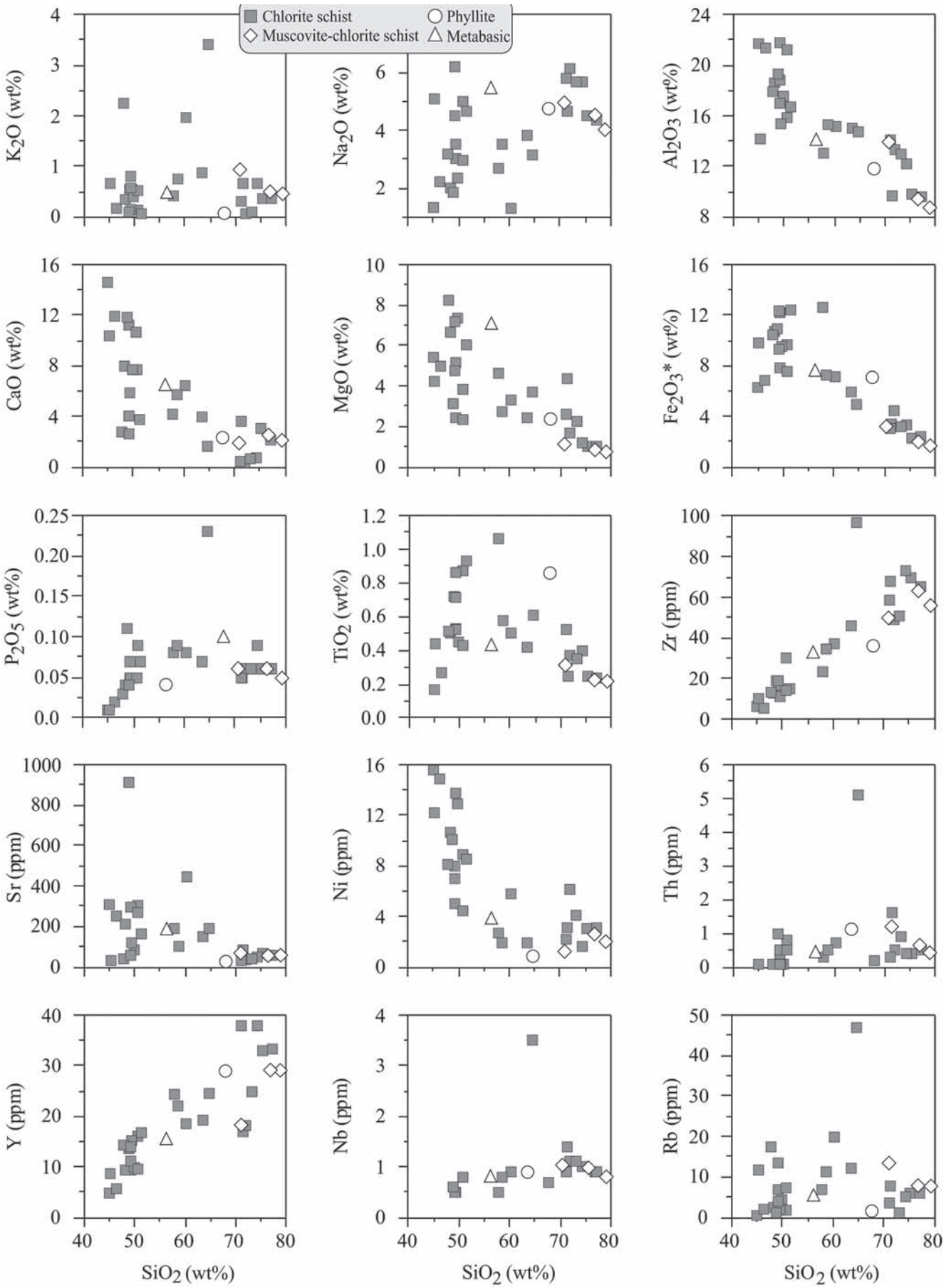


**Fig. 7.** $SiO_2$ versus major oxides (wt%) and trace elements (ppm) variation diagrams for samples from the YMR.

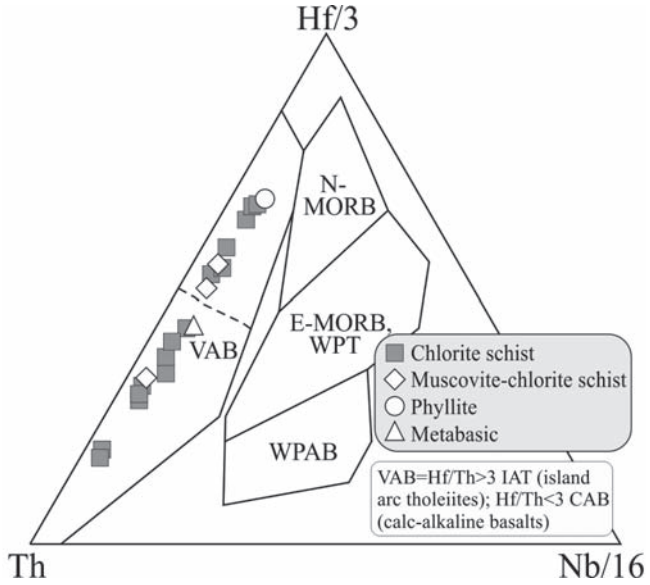


**Fig. 8.** Hf/3-Th-Nb/16 tectonomagmatic discrimination diagram for YMR samples (Wood 1980). N-MORB: N-type mid-ocean ridge basalt, E-MORB: E-type mid-ocean ridge basalt, VAB: volcanic-arc basalt, WPAB: within plate alkaline basalt, WPT: within plate tholeiite.

trends giving ages of 96.1 ± 4.6 Ma (Cenomanian) and 88.8 ± 4.4 Ma (Coniacian), respectively.

Besides, $^{40}Ar$-$^{39}Ar$ dating on plagioclase from the Kızlarkalesi granodiorite, which cuts the YMR, yielded a plateau age of 60.7 ± 4.9 Ma (Selandian) (Aslan et al. 2011).

## 5. Discussion

### 5.1. Pressure and temperature conditions during metamorphism

Mineral assemblages in the greenschist rocks of the YMR are shown in an ACF diagram (Fig. 11). The studied rocks mostly fall in the chlorite zone of mafic source rocks (Best 1982). The Kızlarkalesi granodiorite body emplaced after metamorphism, and caused contact metamorphism in the schists evident by new growth of epidote and garnet.

The mafic rocks of the YMR contain the mineral assemblage albite-chlorite-epidote-calcite which is characteristic for low-grade greenschist facies conditions.

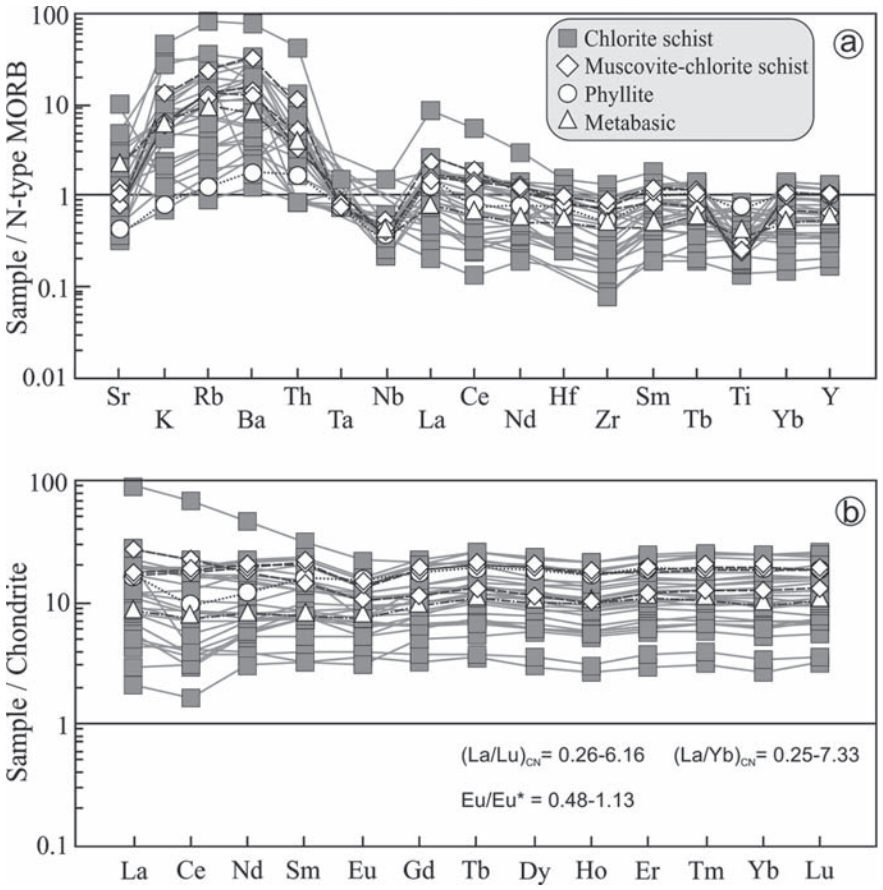


**Fig. 9. (a)** N-type MORB (Sun & McDonough 1989) normalized trace element diagram and **(b)** chondrite normalized (Sun & McDonough 1989) REE diagram of the YMR.

**Table 6.** $^{40}$Ar-$^{39}$Ar analytical data for plagioclase from metabasic rocks of the YMR.

Sample: $M32_1$ (plagioclase-1) J = 0.003465 ± 0.000031

| T °C | $^{40}$Arcc(STP) | $^{40}$Ar/$^{39}$Ar | ± 1σ | $^{38}$Ar/$^{39}$Ar | ± 1σ | $^{37}$Ar/$^{39}$Ar | ± 1σ | $^{36}$Ar/$^{39}$Ar | ± 1σ | Ca/K | ∑$^{39}$Ar (%) | Age (Ma) | ± 1σ |
|---|---|---|---|---|---|---|---|---|---|---|---|---|---|
| 500 | $9.75*10^{-9}$ | 19.76 | 0.04 | 0.0095 | 0.0017 | 0.4649 | 0.0122 | 0.0225 | 0.0020 | 1.7 | 25.5 | 80.24 | 3.68 |
| 650 | $15.16*10^{-9}$ | 19.90 | 0.04 | 0.0205 | 0.0021 | 0.5680 | 0.0050 | 0.0151 | 0.0018 | 2.0 | 64.9 | 93.97 | 3.33 |
| 800 | $8.96*10^{-9}$ | 28.03 | 0.19 | 0.0398 | 0.0055 | 5.3506 | 0.0414 | 0.0415 | 0.0067 | 19.3 | 81.4 | 95.95 | 11.76 |
| 1000 | $8.74*10^{-9}$ | 34.43 | 0.26 | 0.0498 | 0.0125 | 23.3994 | 0.1760 | 0.0727 | 0.0074 | 84.2 | 94.6 | 79.18 | 13.16 |
| 1150 | $6.54*10^{-9}$ | 62.23 | 0.95 | 0.0840 | 0.0139 | 27.2246 | 0.4224 | 0.1664 | 0.0155 | 98.0 | 100.0 | 79.92 | 27.12 |

Sample: $M32_2$ (plagioclase-2) J = 0.003438 ± 0.000031

| T °C | $^{40}$Arcc(STP) | $^{40}$Ar/$^{39}$Ar | ± 1σ | $^{38}$Ar/$^{39}$Ar | ± 1σ | $^{37}$Ar/$^{39}$Ar | ± 1σ | $^{36}$Ar/$^{39}$Ar | ± 1σ | Ca/K | ∑$^{39}$Ar (%) | Age (Ma) | ± 1σ |
|---|---|---|---|---|---|---|---|---|---|---|---|---|---|
| 500 | $11.62*10^{-9}$ | 23.893 | 0.038 | 0.0282 | 0.0021 | 0.525 | 0.028 | 0.0307 | 0.0016 | 1.89 | 21.8 | 89.6 | 2.9 |
| 650 | $20.78*10^{-9}$ | 22.028 | 0.042 | 0.0183 | 0.0016 | 0.617 | 0.014 | 0.0164 | 0.0019 | 2.22 | 64.1 | 103.5 | 3.4 |
| 800 | $9.13*10^{-9}$ | 27.741 | 0.141 | 0.0222 | 0.0037 | 6.460 | 0.046 | 0.0454 | 0.0051 | 23.26 | 78.8 | 86.7 | 8.9 |
| 1150 | $18.74*10^{-9}$ | 39.687 | 0.145 | 0.0452 | 0.0026 | 20.648 | 0.083 | 0.0792 | 0.0036 | 74.33 | 100.0 | 98.4 | 6.4 |

Fig. 12 shows the changes of the mineral paragenesis in the metabasic rocks of the YMR for different temperature and pressure conditions. The average temperature for the greenschist rocks of the YMR was estimated at ~400 °C, with pressures of 4–5 kbar (Gücer 2008). The conditions of progressive regional metamorphism in the greenschist rocks can be related to the plagioclase and amphibole compositions (Bucher & Frey 2002). In our samples, plagioclase from the chlorite schists has albitic composition ($An_{0.17-1.59}$ $Ab_{98.26-99.69}$ $Or_{0.05-0.30}$), as would be expected in greenschist facies rocks. Actinolitic amphibole was formed as a result of pyroxene alteration. Actinolite is typical of low grade metamorphism and changes with increasing metamorphic grade into hornblende (Bucher & Frey 2002). Actinolitic amphibole of the studied rocks yields pressures of 0.2–0.6 (± 0.6) kbar (Schmidt 1992) or 0.4–0.9 (± 1) kbar (Hollister et al. 1987).

Chlorite is a typical product of low-grade metamorphism in rocks of basic composition (Potel 2007). In the chlorite schists, the chlorites are commonly found in association with epidote, albite, quartz and sericite. Chlorites from the metabasic rocks plot in the ripidolite–picnochlorite field (Fig. 13a) which argues for a volcanic origin (Zane et al. 1998). In the ($Al^{VI}$+2Ti+Cr) versus $Al^{IV}$ diagram, chlorites from the metabasic rocks plot in the lower part, within a rectangular field (Fig. 13b), again supporting the idea that their composition relates to the metabasic character of the parental rock. In addition, chlorites of the metabasic rocks fall in the Type I field in the Al–Fe–Mg triangular diagram (Fig. 13c). Their Mg-rich compositione provides corroborating evidence for a volcanic origin (Zane & Weiss 1998, Bailey 1980).

Chlorites are well-suited to determine the thermobarometric conditions during low-grade metamorphism. Chlorite thermometry based on the methods of Cathelineau & Nieva (1985) and Cathelineau (1988) and Jowett (1991) yields temperatures between 320–347 °C. Pressures are calculated at about 4 kbars, indicating a burial depth of approximately 15 km.

## 5.2. Potential protoliths and geodynamic implications

Low-grade metamorphic rocks can form in different geological settings, including subduction zones, continental orogens, volcanic arcs and ocean ridges (Frey & Robinson 1999). From Late Cretaceous to Upper Paleogene the Eastern Pontides constituted a complex tectonic regime (Okay & Şahintürk 1997). The Neo-Tethys was already subducting under the Pontides in the Early Cretaceous (ca. 105 Ma, Okay et al. 2006). The magmatic arc started to develop in the Late Cretaceous as a result of the oceanic subduction along the İzmir-Ankara-Erzincan suture zone (Turonian, ca. 90 Ma, Okay & Şahintürk 1997, Okay 2008). Late Cretaceous volcanic rocks, best exposed in the Eastern Pontides, consist of a sequence of submarine lavas and pyroclastic rocks with intercalated sediments (Okay 2008). The geochemical composition of the greenschist rocks resembles calc-alkaline arc volcanics. LILEs-HFSEs and concentrations of other trace elements, such as Sr, Ta, Ce, Hf, Sm, Y and Yb are similar to MORB, whereas the negative Ta and Nb anomaly emphasises the influence of a subduction zone. Enrichment

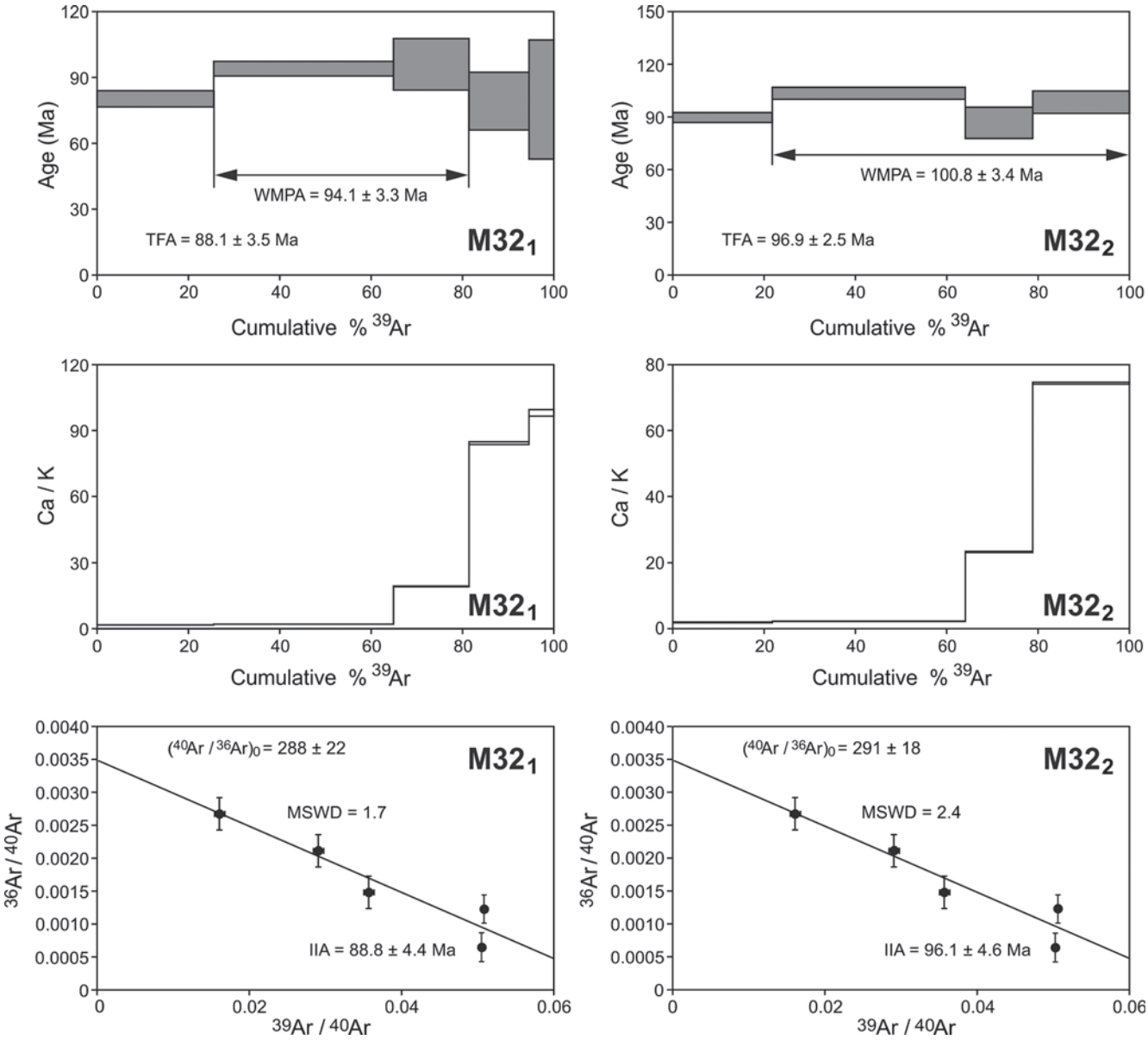


**Fig. 10.** $^{40}$Ar-$^{39}$Ar age spectra (top panels), Ca/K spectrum (middle panels) and inverse isochron diagrams (bottom panels) for plagioclase separates of the YMR. Grey boxes in the spectra and black dots in the inverse isochron diagrams represent steps included in age calculation. **WMPA** = weighted mean plateau age, **MSWD** = mean square weighted deviation, **TFA** = total fusion age, **Ca/K** = apparent Ca/K ratio, **IIA** = inverse isochron age, **M32$_1$** and **M32$_2$** = sample no.

in LILEs (e.g. Sr, $K_2O$, Rb, and Ba), and Th may indicate that the parental magmas were derived from a lithospheric mantle source (Pearce & Peate 1995, Elburg et al. 2002, Zellmer et al. 2005). The depletion of Nb and Ta relative to LILEs in the studied rocks is a feature of arc magmas imposed by fluids derived from the subducted slab or sediments (Wakesworth et al. 1997, Elburg et al. 2002).

The Ar-Ar plagioclase ages from the two metabasic rocks (100.8 ± 3.4, 94.1 ± 3.3 Ma are in line with the 95–90 Ma old blueschist rocks exposed along the İzmir-Ankara-Erzincan and Amassia-Stepanavan suture zones (Caucasus) confirming the subduction of oceanic crust during the Late Cretaceous (Rolland et al. 2009, Oberhänsli et al. 2011).

The Refahiye ophiolite tectonically overlies the studied YMR. It is one of the best exposures of oceanic lithosphere and related to subduction of the Neo-Tethys. The ophiolite was emplaced by north-directed backthrusting onto the Pontides in the Late Cretaceous (Sarifakioğlu et al. 2009). Closure of the Neo-Tethyan ocean caused a collision between the Pontide arc and the Tauride-Anatolide platform. This collision started along the İzmir-

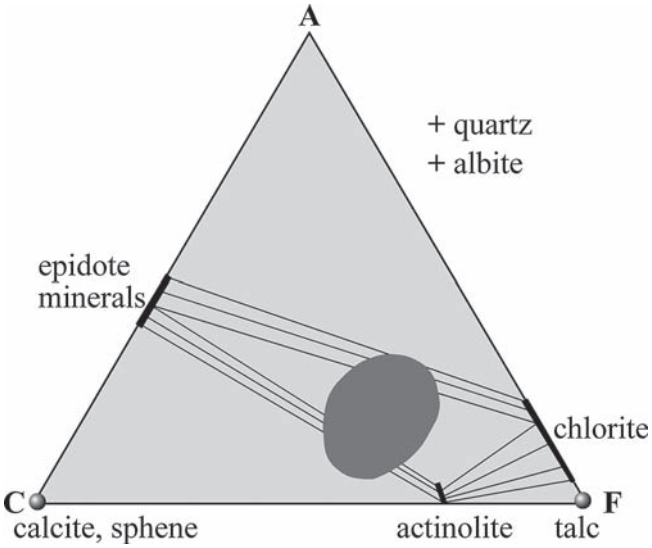


**Fig. 11.** ACF diagram showing the metamorphic mineral assemblages of the greenschist rocks from the YMR (Best 1982). **A** = $Al_2O_3$+$Fe_2O_3$+-($Na_2O$+$K_2O$); **C** = CaO-3,3 $P_2O_5$; **F** = FeO+MgO+MnO.

Ankara-Erzincan suture zone about 65 Ma ago (Okay & Şahintürk 1997). During the Late Cretaceous effusive volcanism was accompanied by the emplacement of large calc-alkaline plutons (e.g., Aslan 2005). The calc-alkaline Kızlarkalesi granodiorite (Gücer 2008) formed during the collision period and emplaced into the YMR around 60.7 ± 4.9 Ma (Selandian – Late Paleocene).

The YMR were originally composed of volcano-sedimentary rocks. These rocks consisting of basalts/andesites, claystones and argillaceous limestone were subjected to low-grade greenschist metamorphism during subducting of the Neo-Tethys below the Pontides. The YMR were metamorphosed around 90–70 Ma (Late Cretaceous) prior to the emplacement of the Kızlarkalesi granodiorite body. At the same time greenschist facies rocks were formed along to İzmir-Ankara-Erzincan suture zone and the Caucasus (Rolland et al. 2009, Oberhänsli et al. 2011).

## 6. Conclusions

Geochemical characteristics of the YMR, such as negative Nb anomalies, indicate volcanic-arc affinities. The rocks are enriched in Th, K and Rb, pointing to the involvement of crustal material. The protoliths of the YMR developed in a volcanic-arc setting, where basic volcanic rocks, their pyroclastic equivalents and other sedimentary rocks such

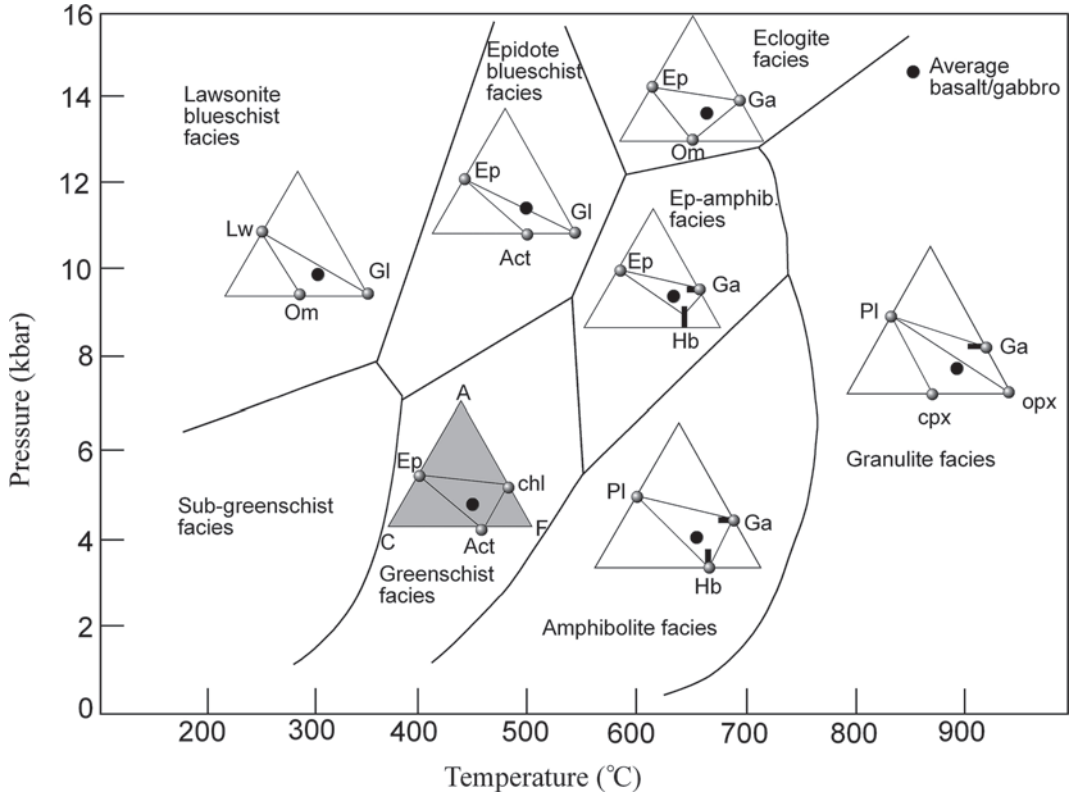


**Fig. 12.** Pressure-temperature plot showing metamorphic mineral assemblages of basic rocks represented by ACF diagrams (Bucher & Frey 2002). Grey-shaded triangle shows mineral assemblage in YMR.

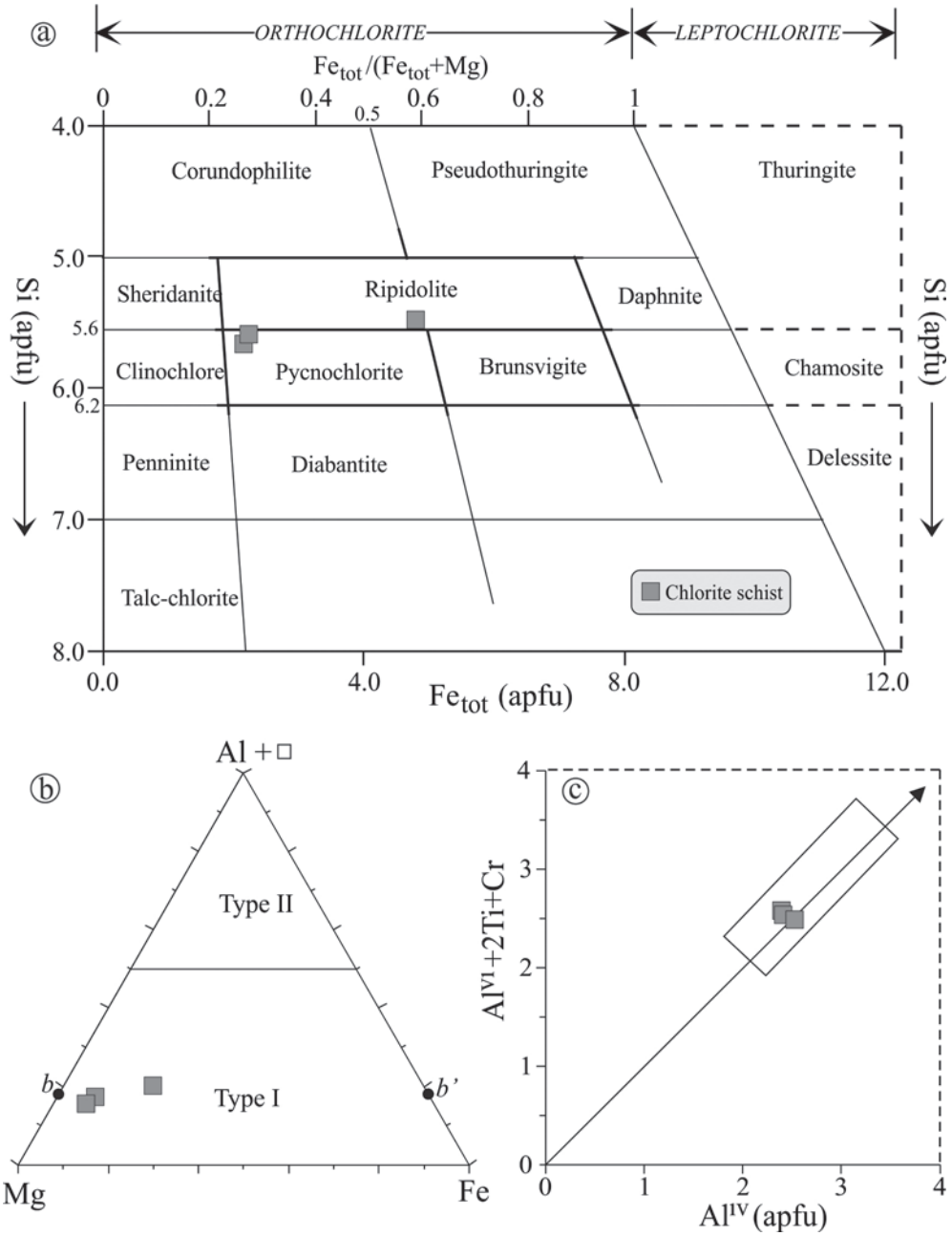


**Fig. 13. (a)** Si-$Fe_{tot}$ chlorite classification diagram (Hey 1954), **(b)** chlorite discrimination diagram (Bailey 1980, Zane & Weiss 1998), **(c)** ($Al^{VI}$+2Ti+Cr) versus $Al^{IV}$ diagram of metabasic rocks from YMR (Zane et al. 1998).

as claystone and limestone were formed. Regional metamorphism of the YMR occurred during late Cretaceous subduction of the Neo-Tethys under the Pontide belt. The YMR were metamorphosed under greenschist facies conditions between 90–70 Ma at ~320–350 °C and 4 kbars. Following this metamorphism, the rocks were obducted onto older continental crust of the Eastern Pontides. The YMR are cut by a granitic body which has imposed contact metamorphism which postdates regional metamorphism of the YMR by ca. 20 Ma.

## Acknowledgements

This article is derived from the MSc thesis of the first author. The study was financially supported by the Karadeniz Technical University Scientific Research Fund. The authors thank Wolfgang Siebel for general improvement of the manuscript and Heinz-Günter Stosch for his editorial input. Special thanks to Mehmet Arslan and Aral Okay for constructive criticism, Ömer Bozkaya and Bektas Uz for reviews. Thanks also go to Lang Shi for per-

forming the microprobe analyses at McGill University, Canada. Aaron Stallard improved the English of the manuscript.

## References


Altinkaynak, L. (2001): Ağvanis masifi doğu kesimi ve çevre kayaçlarının jeolojisi, petrografisi ve jeokimyası. – Ph D. Thesis, Karadeniz Technical University Science Ens. 290 pp.

Aslan, Z. (2005): Petrography and petrology of the calc-alkaline Sarıhan Granitoid (NE Turkey): An example of magma mingling and mixing. – Turk. J. Earth Sci. **14**: 185–207.

Aslan, Z., Gücer, M. A. & Arslan, M. (2011): $^{39}$Ar-$^{40}$Ar dating on plagioclases of metabasic and metagranitic rocks in the Yoncayolu metamorphics, NE Turkey. – 21st V. M. Goldschmidt Conference, Mineral. Mag. **75**,3: p. 460.

Ayan, M. (1973): Migmatites in the Gördes area. – Bull. Miner. Res. Explor. Inst. Turk. **81**: 85–109.

Bailey, S. W. (1980): Structures of layer silicates. – In: Brindley, G. W. & Brown, G. (Eds.): Crystal structures of clay minerals and their X-ray identifications. Miner. Soc. London, 2–123.

Bektaş, O. (1981): Kuzey Anadolu fay zonunun Erzincan-Tanyeri bucağı yöresindeki jeolojik özellikleri ve yerel ofiyolit sorunları. – PhD Thesis, Karadeniz Technical University Science Ens., 196 pp.

Best, M. G. (1982): Igneous and metamorphic petrology. – Freeman, San Francisco, USA, 458 pp.

Bucher, K. & Frey, M. (2002): Petrogenesis of metamorphic rocks. – Springer, 341 pp.

Cathelineau, M. (1988): Cation site occupancy in chlorites and illites as a function of temperature. – Clay Miner. **23**: 471–485.

Cathelineau, M. & Nieva, D. (1985): A chlorite solid solution geothermometer; The Los Azufres (Mexico) geothermal system. – Contrib. Mineral. Petrol. **91**: 235–244.

Elburg, M. A., Bergen, M. V., Hoogewerff, J., Foden, J., Vroon, P., Zulkarnain, I. & Nasution, A. (2002): Geochemical trends across an arc-continent collision zone: magma sources and slab-wedge transfer processes below the Pantar Strait volcanoes, Indonesia. – Geochim. Cosmochim. Acta **66**: 2771–2789.

Eyüboglu, Y., Bektaş, O., Seren, A., Nafiz, M., Jacoby, W. R. & Özer, R. (2006): Three-directional extensional deformation and formation of the Liassic rift basins in the eastern Pontides (NE Turkey). – Geol. Carpath. **57**: 337–346.

Frey, M. & Robinson, D. (1999): Low-grade metamorphism. – Blackwell Science, London, 313 pp.

Göncüoğlu, M. C. & Turhan, N. (1983): New results on the age of Bitlis metamorphics. – Bull. Miner. Res. Explor. Inst. Turk. **95**: 1–5.

Gücer, M. A. (2008): Yonyayolu metamorfitleri (Erzincan-Üzümlü) ve çevre kayaçlarının mineralojik, petrografik ve jeokimyasal incelenmesi. – Ms Thesis, Karadeniz Technical University Science Ens., 125 pp.

Hawkesworth, C. J., Turner, S. P., Mcdermott, F., Peate, D. W. & Van Calsteren, P. (1997): U-Th isotopes in arc magmas: implications for element transfer from the subducted crust. – Science **276**: 551–555.

Hey, M. H. (1954): A new review of the chlorites. – Mineral. Mag. **30**: 277–292.

Hollister, L. S., Grisson, G. C., Peters, E. K., Stowell, H. H. & Sisson, V. B. (1987): Confirmation of the empirical calibration of Al in hornblende with pressure of solidification of calc-alkaline plutons. – Am. Mineral. **72**: 231–239.

Jowett, E. C. (1991): Fitting iron and magnesium into the hydrothermal chlorite geothermometer. – GAC/MAC/SEG Joint Annual Meet 16: A62.

Keskin, M. (2003): Magma generation by slab steepening and breakoff beneath a subduction-accretion complex: An alternative model for collision-related volcanism in Eastern Anatolia, Turkey. – Geophys. Res. Lett. **30**: 1–4.

Ketin, I. (1966): Anadolu'nun tektonik birlikleri. – Bull. Miner. Res. Explor. Inst. Turk. **66**: 20–34.

Leake, E. B., Wooley, A. R., Arps, C. E. S., Birch, W. D., Gilbert, M. C., Grice, J. D., Hawthorne, F. C., Kato, A., Kisch, H. J., Krivovichev, V. G., Linthout, K., Laird, J., Mandarino, J., Maresch, W. V., Nickhel, E. H., Rock, N. M. S., Schumacher, J. C., Smith, D. C., Stephenson, N. C. N., Ungaretti, L., Whittaker, E. J. W. & Youzhi, G. (1997): Nomenclature of amphiboles: Report of the subcommittee on amphiboles of the international mineralogical association, commission on new minerals and mineral names. – Am. Mineral. **82**: 1019–1037.

Oberhänsli, R., Bousquet, R., Candan, O. & Okay, A. I. (2012): Dating subduction events in east Anatolia, Turkey. – Turk. J. Earth Sci. **21**: 1–17.

Okay, A. I. (1984): The geology of the Ağvanis metamorphic rocks and neighbouring formations. – Bull. Miner. Res. Explor. Inst. Turk. **99**: 16–36.

Okay, A. I. (1989): Tectonic units and sutures in the Pontides, northern Turkey. In: Şengör, A. M. C. (Eds.): Tectonic evolution of the Tethyan region. – Kluwer Academic Publ. Dordrecht, 109–115.

Okay, A. I. (2008): Geology of Turkey: a synopsis. – Anschnitt **21**: 19–42.

Okay, A. I. & Tüysüz, O. (1999): Tethyan sutures of northern Turkey. – In: Durant, B., Jolivet, F., Horvath, F. & Seranne, M. (Eds.): The Mediterranean basin: Tertiary extension within the Alpine orogen. – J. Geol. Soc. London **156**: 475–515.

Okay, A. I. & Şahintürk, O. (1997): Geology of the eastern Pontides. In: Robinson, A. G. (Eds.): Regional and petroleum geology of the Black Sea and surrounding. – AAPG Mem. **68**: 291–311.

Okay, A. I. & Satir, M. (2000): Coeval plutonism metamorphism in a latest Oligocene metamorphic core complex in northwest Turkey. – Geol Mag. **137**: 495–516.

Okay, A. I. & Göncüoğlu, M. C. (2004): Karakaya complex: a review of data and concepts. – Turk. J. Earth Sci. **13**: 77–95.

Okay, A. I., Tüysüz, O., Satir, M., Özkan-Altiner, S., Altiner, S., Altiner, D., Sherlock, S. & Eren, R. H. (2006): Cretaceous and Triassic subduction-accretion, HP/LT metamorphism and continental growth in the Central Pontides, Turkey. – Geol. Soc. Am. Bull. **118**: 1247–1269.

Pearce, J. A. & Peate, D. W. (1995): Tectonic implications of the composition of volcanic arc magmas. – Ann. Rev. Earth Planet Sci. Lett. **23**: 251–285.

Potel, S. (2007): Very low grade metamorphic study in the pre-Late Cretaceous terranes of New Caledonia (southwest Pasific Ocean). – Isl. Arc **16**: 291–305.

Rolland, Y., Billo, S., Corsini, M., Sosson, M. & Galoyan, G. (2009): Blueschists of the Amassia-Stepanavan suture zone (Armenia): linking Tethys subduction history from E-Turkey to W-Iran. – Int. J. Earth Sci. **98**: 533–550.

Ross, P. S. & Bédard, J. H. (2009): Magmatic affinity of modern and ancient subalkaline volcanic rocks determined from trace-element discriminant diagrams. – Can. J. Earth Sci. **46**: 823–839.

Sarifakioglu, E., Ozen, H. & Winchester, J. A. (2009): Petrogenesis of the Refahiye ophiolite and its tectonic significance for Neotethyan ophiolites along the İzmir-Ankara-Erzincan suture zone. – Turk. J. Earth Sci. **18**: 187–207.

Schmidt, M. W. (1992): Amphibole composition in tonalite as a function of pressure: an experimental calibration of the Al in hornblende barometer. – Contrib. Mineral. Petrol. **110**: 304–310.

Sun, S. S. & Mcdonough, W. F. (1989): Chemical and isotopic systematics of oceanic basalts: implications for mantle composition and processes. – In: Saunders, A. D. & Norry, M. J. (Eds.): Magmatism in the Ocean Basins. J. Geol. Soc. London. Spec. Pub. **42**: 313–345.

Şengör, A. M. C. & Yilmaz, Y. (1981): Tethyan evolution of Turkey: a plate tectonic approach. – Tectonophysics **75**: 181–241.

Şengör, A. M. C., Görüs, N. & Şaroglu, F. (1985): Strike-slip faulting and related basin formation in zones of tectonic escape: Turkey as a case study. – In: Biddle, K. T. & Christie-Blick, N. (Eds.): Strike-slip deformation, basin formation and sedimentation. Soc. Eco. Paleontol. Mineral. Spec. Publ. **37**: 227–264.

Şengör, A. M. C., Özeren, S., Genç, T. & Zor, E. (2003): East Anatolian high plateau as a mantle-supported, north–south shortened domal structure. – Geophys Res. Lett. **30** (24): 8045.

Topuz, G., Altherr, R., Satir, M. & Schwarz, W. (2004): Low grade metamorphic rocks from the Pulur complex, NE Turkey: Implications for pre-Liassic evolution of the eastern Pontides. – Int. J. Earth Sci. **93**: 72–91.

Topuz, G., Altherr, R., Schwarz, H. W., Dokuz, A. & Meyer, H. P. (2007): Variscan amphibolite-facies rocks from the Kurtoğlu metamorphic complex, Gümüşhane area, Eastern Pontides, Turkey. – Int. J. Earth Sci. **96**: 861–873.

Topuz, G., Okay, A. I., Altherr, R., Schwarz, H. W., Siebel, W., Zack, T., Satir, M. & Şen, C. (2011): Post-collisional adakite-like magmatism in the Agvanis massif and implications for the evolution of the Eocene magmatism in the eastern Pontides (NE Turkey). – Lithos **125**: 131–150.

Winchester, J. A. & Floyd, P. A. (1977): Geochemical discrimination of different magma series and their differentiation products using immobile elements. – Chem. Geol. **20**: 97–127.

Winchester, J. A., Park, R. G. & Holland, J. G. (1980): The geochemistry of Lewisian semipelitic schists from the Gairloch district, wester Ross. – Scott. J. Geol. **16**: 165–179.

Wood, D. A. (1980): The application of a Th-Hf-Ta diagram to problems of tectonomagmatic classification and to establishing the nature of crustal contamination of basaltic lavas of the British Tertiary volcanic province. – Earth Planet. Sci. Lett. **50**: 11–30.

Zane, A. & Weiss, Z. (1998): A procedure for classifying rock-forming chlorites based on microprobe data. – Rend. Fis. Acc. Lincei **9**: 51–56.

Zane, A., Sassi, R. & Guidotti, C. V. (1998): New data on metamorphic chlorite as a petrogenetic indicator mineral, with special regard to greenschist-facies rocks. – Can. Mineral. **36**: 713–726.

Zellmer, G. F., Annen, C., Charlier, B. L. A., George, R. M. M., Turner, S. P. & Hawkesworth, C. J. (2005): Magma evolution and ascent at volcanic arcs: constraining petrogenetic processes through rates and chronologies. – J. Volcanol. Geotherm. Res. **140**: 171–191.

Manuscript received: October 22, 2013.; accepted: March 8, 2014.
Responsible editor: W. Siebel

**Authors' addresses:**

Mehmet Ali Gücer, Department of Geology, Gümüşhane Engineering Faculty, Gümüşhane University, Gümüşhane 29000, Turkey, E-mail: maligucer@gmail.com

Zafer Aslan, Department of Geology, Engineering & Architecture Faculty, Balıkesir University, Balıkesir 10145, Turkey, E-mail: zaslan@balikesir.edu.tr